Journal of Molecular Structure 1294 (2023) 136448

Contents lists available at ScienceDirect

Journal of Molecular Structure

journal homepage: www.elsevier.com/locate/molstr

Novel azole-urea hybrids as VEGFR-2 inhibitors: Synthesis, *in vitro* antiproliferative evaluation and *in silico* studies

Mohammad Musa Shirzad [a], Necla Kulabaş [b], Ömer Erdoğan [c], Özge Çevik [d], Damla Dere [e], Kemal Yelekçi [e], Özkan Danış [a,*], İlkay Küçükgüzel [f,*]

[a] Department of Chemistry, Faculty of Science, Marmara University, İstanbul 34722, Türkiye
[b] Department of Pharmaceutical Chemistry, Faculty of Pharmacy, Marmara University, İstanbul 34854, Türkiye
[c] Department of Medical Biochemistry, Medical Faculty, Gaziantep Islam Science and Technology, Gaziantep 27010 Türkiye
[d] Department of Biochemistry, Faculty of Medicine, Adnan Menderes University, Aydın 09010 Türkiye
[e] Department of Bioinformatics and Genetics, Faculty of Engineering and Natural Sciences, Kadir Has University, İstanbul, Türkiye
[f] Department of Pharmaceutical Chemistry, Faculty of Pharmacy, Fenerbahçe University, İstanbul 34758, Türkiye

ARTICLE INFO

Keywords:
VEGFR-2 inhibitor
Anti-cancer
Pyrazole
1,3,4-oxadiazoles
1,3,4-thiadiazoles
1,2,4-triazole-3-thione

ABSTRACT

The vascular endothelial growth factor receptor-2 (VEGFR-2) is a receptor tyrosine kinase known to be abnormally expressed in various malignant tumors, including breast cancer, and is considered one of the most important contributors to tumor angiogenesis. Sorafenib is one of many VEGFR-2 inhibitors that have received approval for clinical use from the US FDA in recent years. Accordingly, in this study, the synthesis of two new pyrazoles, six 1,3,4-oxadiazoles, four 1,3,4-thiadiazoles, and ten 1,2,4-triazole-3-thione derivatives having structural characteristics similar to sorafenib was carried out. A preliminary screening of synthesized compounds and known inhibitors sorafenib and staurosporine at 10 μM concentration on *in vitro* activity of VEGFR-2 was performed, and compounds **10c, 8a**, and 11 g were identified as the most potent derivatives with% VEGFR-2 residual activities lower than 30%, and dose-dependent inhibition studies was carried out to determine the IC_{50} values of these inhibitors. Compound **10c** was found to be the most potent inhibitor of VEGFR-2 activity with an IC_{50} value of 0.664 μM. The anti-proliferative activity of synthesized derivatives was assessed against a breast carcinoma (MCF-7) cell line, a triple negative human breast adenocarcinoma (MDA-MB-231) cell line, and noncancerous fibroblast cells (L929). Compound **8a** displayed superior activity when compared to sorafenib against MCF-7 (7.69 fold) and MDA-MB-231 (1.52 fold) cell lines while displaying 3.75-fold less toxicity against the normal L929 cell line. Annexin V binding assay revealed that compound **8a** significantly increased early and late apoptosis in MCF-7 cells and late apoptosis and necrosis in MDA-MB-231 cells. Computational studies such as molecular docking and ADMET evaluation were performed to elucidate the binding interactions and drug-likeness of the synthesized compounds. The results indicate that compound **8a** could be a promising candidate for the development of a novel anti-angiogenic and anti-proliferative agent.

1. Introduction

Cancer is known as one of the deadly diseases globally and still remains as a major burden of disease and human health. Based on a WHO (World Health Organization) report in 2020, 10 million deaths occurred due to this disease worldwide (https://www.who.int/news-room/fact-sheets/detail/cancer). Breast cancer is the most common cancer observed and accounts for nearly one-third of female cancer patients [1]. Currently, the most common ways for cancer treatments are surgery, radiotherapy, and chemotherapy. However, use of non-selective chemotherapeutic agents in chemotherapy, lower the responses of patients and increase the chance of developing resistances against these drugs [2]. In the light of this fact, developing novel drugs that inhibit the proliferation of cancer cells without any or lower side effects on healthy cells has become crucial to ease the burden of cancer.

The process by which new blood vessels develop from pre-existing ones is known as angiogenesis and is an essential physiological process for wound healing, tissue repair, and female reproductive health. Several diseases, including diabetes, atherosclerosis, rheumatoid arthritis, and cancer, are correlated with the regulated angiogenesis and

* Corresponding authors.
E-mail addresses: odanis@marmara.edu.tr (Ö. Danış), ilkay.kucukguzel@fbu.edu.tr (İ. Küçükgüzel).

https://doi.org/10.1016/j.molstruc.2023.136448
Received 1 July 2023; Received in revised form 16 August 2023; Accepted 17 August 2023
Available online 18 August 2023

lymphangiogenesis [3]. However, angiogenesis is also an important characteristic of both breast cancer and malignancies in general. Tumors can promote angiogenesis by secreting numerous chemical signals, such as adhesion, growth, and transcription factors, cytokines, and other signaling molecules [4].

Protein tyrosine kinases (PTKs) are enzymes that catalyze the transfer of the phosphate group from ATP to target proteins [5]. PTKs are important regulators of cellular processes such as proliferation, survival, apoptosis, metabolism, transcription, differentiation, and angiogenesis, and these processes are responsible for various diseases such as cardiovascular disease, inflammation, neurodegenerative diseases, and cancer [6,7]. The main regulator of tumor angiogenesis, vascular endothelial growth factor receptor 2 (VEGFR-2), is a receptor-tyrosine kinase known as KDR in human epithelial cells [8]. The interaction of its ligand VEGF with VEGFR-2 results in homo- and heterodimerization of VEGFR-2, and consequent phosphorylation of the receptor eventually leads to endothelial cell survival, proliferation, migration, and vascular permeability [9]. Due to hypoxia-inducible factors, transcription factors drastically enhance the rate of gene transcription and improve the stability of VEGF mRNA in cancer cells, which causes the expression of the VEGF gene to increase. Other growth factors, namely placental growth factor, epidermal growth factor, and cytokines, also have an impact on the upregulation of VEGF mRNA [3]. Furthermore, VEGFR-2 is only weakly expressed in healthy tissue or cells and it has been demonstrated that 64.5% (91/141) of invasive breast carcinomas overexpress VEGFR-2 [10]. In light of these findings, the development of small-molecule tyrosine kinase inhibitors (TKIs) that bind the ATP binding site of VEGFR-2 and thus prevent angiogenesis in tumor cells emerges as an important approach for the generation of safe and selective anticancer agents.

The US Food and Drug Administration (FDA) has approved 64 small-molecule kinase inhibitors as of 2021 for the treatment of malignancies, including breast cancer, renal cell carcinoma, hepatocellular carcinoma, and neuroendocrine tumors [11]. Currently, there are nine VEGFR-2 targeted small molecule inhibitors (sorafenib, sunitinib, pazopanib, vandetanib, axitinib, regorafenib, cabozantinib, lenvatinib, and tivozanib) approved by the US FDA as anticancer agents for clinical use [12,13]. The structure, approval date, and IC_{50} values for VEGFR-2 of these inhibitors are given in Fig. 1.

PTK inhibitors classified based on their binding site and bound PTK conformation. Usually, PTK inhibitors can be classified into 3 types (I, II, and III). Type I and II are competitive inhibitors that bind to the ATP binding pocket, the difference is that type I binds to the PTK active conformation (DFG-in), while type II binds to an inactive conformation (DFG-out), and type III are non-competitive inhibitors (allosteric inhibitors) that bind in a distinct site from the active site in the ATP binding pocket [14,15].

Among VEGFR-2 inhibitors, Sorafenib, a multikinase inhibitor, is a member of type II inhibitors, which inhibit the PTKs involved in angiogenesis (VEGFR-1, 2, and 3 and PDGFRβ) and tumorigenesis (Flt-3, c-Kit, and RET). Sorafenib possesses four important pharmacophoric features: a heteroaromatic moiety that occupies the hinge region (ATP-binding domain) by interaction with GLU917 and/or CYS919 residues; an aryl linker to locate or fit into the area between the ATP-binding domain and DFG domain; an important urea moiety to produce hydrogen bonds with CYS919, GLU885, and ASP1046 residues in the DFG domain; and a lipophilic group (4-chloro-3-(trifluoromethyl)-phenyl) to produce a hydrophobic interaction in the allosteric region of the inactive confirmation of the receptor (Fig. 2) [16]. Although sorafenib has a good potency, selectivity, and tolerable safety profile, its water solubility is weak and its oral bioavailability is quite low [17]. Drug resistance, toxicities, and the cost of therapy are the main problems and challenges for cancer patients. To overcome these problems, the priority is to produce or develop new and selective small molecule PTK inhibitors with different mechanism of actions (multikinase inhibitors) to bind with more than one target (protein tyrosine kinase) and reduce the toxicities and side effects, increase the efficacy, and of course decrease the costs of treatments [16,18]. In order to discover potent new agents with better efficacy and lower toxicity, molecular hybridization approaches, which combine biologically active pharmacophores via a

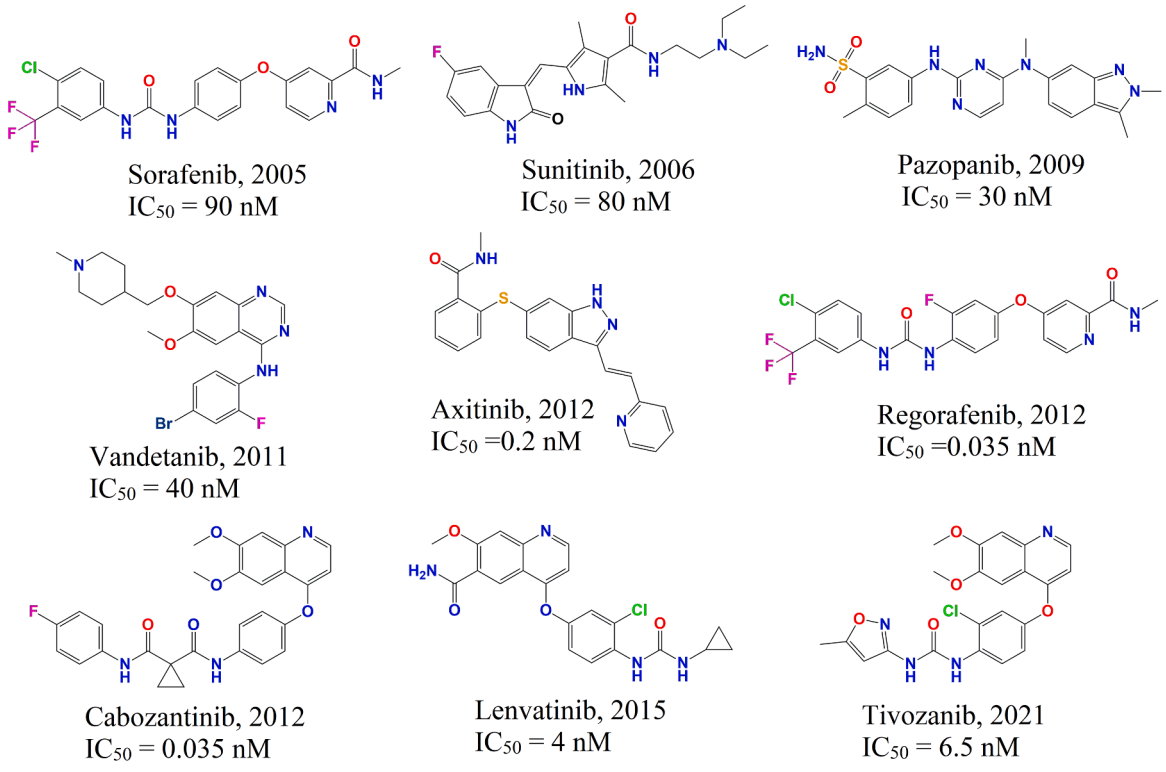

Fig. 1. The structure, approval date, and IC_{50} values for VEGFR-2 of US FDA approved small molecule inhibitors [13].

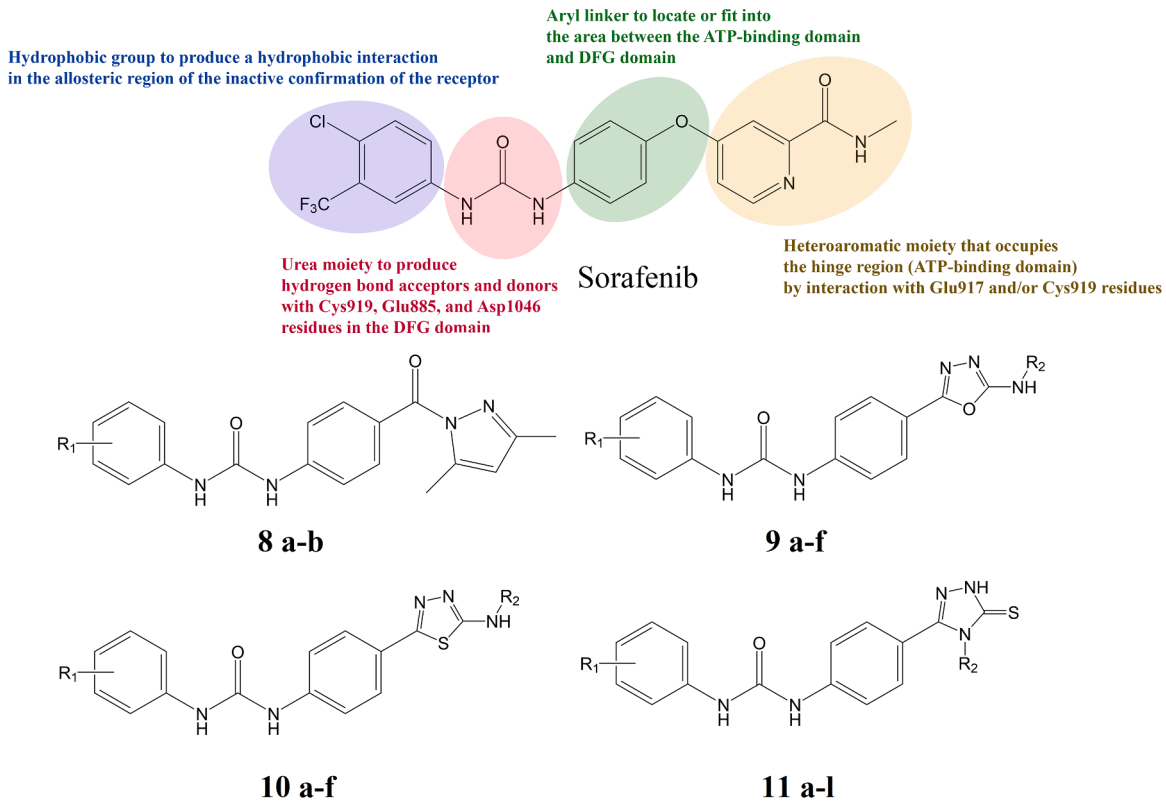

Fig. 2. Chemical structures of our newly designed scaffolds and important pharmacophoric features of sorafenib.

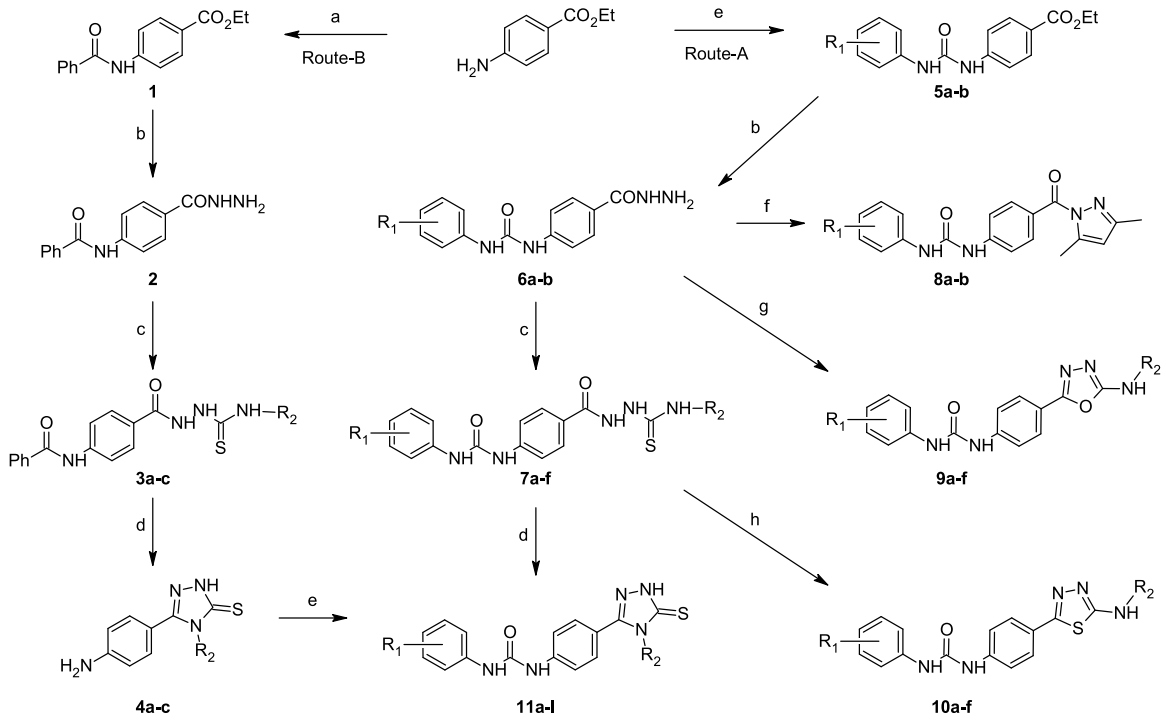

Scheme 1. Synthetic route to target compounds **8a-b, 9a-f, 10a-f** and **11a-l**. Key to reagents: **a.** PhCOCl, Et_2O, rt; **b.** $NH_2NH_2.H_2O$, EtOH, reflux; **c.** R_2NCS, EtOH, reflux; **d.** 2 N NaOH, reflux,%10 HCl; **e.** R_1NCO, DCM, rt; **f.** 2,4-dioxopentane, EtOH, reflux; **g.** 1) R_2NCS, DMSO, rt, 2) $KHSO_4$, DMSO, rt; **h.** H_2SO_4, reflux. **11a-f** were synthesized via Route-A, whereas **11g-l** were synthesized via Route-B.

3a, 4a, R_2: Me, **3b, 4b**, R_2: Et, **3c, 4c**, R_2: Pr, **5a, 6a, 8a**, R_1: H, **5b, 6b, 8b**, R_1: 4-Cl, **9a**, R_1: H, R_2: Me, **9b**, R_1: H, R_2: Et, **9c**, R_1: H, R_2: Pr, **9d**, R_1: 4-Cl, R_2: Me, **9e**, R_1: 4-Cl, R_2: Et, **9f**, R_1: 4-Cl, R_2: Pr, **10a**, R_1: H, R_2: Me, **10b**, R_1: H, R_2: Et, **10c**, R_1: H, R_2: Pr, **10d**, R_1: 4-Cl, R_2: Me, **10e**, R_1: 4-Cl, R_2: Et, **10f**, R_1: 4-Cl, R_2: Pr, **7a, 11a**, R_1: H, R_2: Me, **7b, 11b**, R_1: H, R_2: Et, **7c, 11c**, R_1: H, R_2: Pr, **7d, 11d**, R_1: 4-Cl, R_2: Me, **7e, 11e**, R_1: 4-Cl, R_2: Et, **7f, 11f**, R_1: 4-Cl, R_2: Pr, 11 g, R_1: 3-CF_3, R_2: Me, 11 h, R_1: 3-CF_3, R_2: Et, **11i**, R_1: 3-CF_3, R_2: Pr, **11j**, R_1: 4-CF_3, R_2: Me, **11k**, R_1: 4-CF_3, R_2: Et, **11l**, R_1: 4-CF_3, R_2: Pr

spacer or linker, are usually employed. Using a hybrid molecule to interact with different targets instead of a drug cocktail approach has proven advantageous in terms of preventing unintended drug-drug interactions and determining the effective dosage [19].

In the present work, we follow up on a hybridization plan between an FDA-approved VEGFR-2 inhibitor, sorafenib, and our newly synthesized compounds (Fig. 2). First, we conjugated four different heteroaromatic moieties such as 1,3,4-oxadiazole, 1,3,4-thiadizole, 1,3,4-trizole, and pyrazole with diarylurea core to find their role in the interaction with VEGFR-2 and whether they may interact potently with the important residues (Glu917 and/or Cys919) in the Hinge region. Secondly, the presence of urea as an effective hydrogen bond acceptor and donor in sorafenib encouraged us to design our new synthesized compounds to possess a urea moiety. Third, the phenoxy group plays a significant role in sorafenib, so we designed it as an aryl linker in all our new synthesized derivatives. Finally, as hydrophobic moieties, we preferred phenyl, 4-chlorophenyl, 3-trifluorophenyl, and 4-trifluorophenyl. The inhibitory effects of 26 newly synthesized compounds and sorafenib on VEGFR-2 activity were determined, and their anti-proliferative activity was evaluated *in vitro* against breast carcinoma and breast adenocarcinoma cell lines as well as non-cancerous fibroblast cells. A docking study was also performed to determine the pattern of these drugs' binding inside the VEGFR-2 active site. Additionally, the *in silico* ADME study was used to predict the pharmacokinetic characteristics and drug-likeness properties of the synthesized compounds.

2. Results and discussion

2.1. Chemistry

The synthetic strategies adopted to achieve the target compounds are shown in Scheme 1. For all synthetic work, the starting material was benzocaine. For the synthesis of 1,2,4-triazole series, two different routes were utilized. Route-B started with protection of amine function of benzocaine benzoylation yielding compound **1**, which was then converted to the corresponding hydrazide **2**. Addition of **2** to methyl, ethyl or propyl isothiocyanates gave thiosemicarbazides **3a-c**. Heating the thiosemicarbazides **3a-c** in the presence of sodium hydroxide resulted in both the formation of 1,2,4-triazoles **4a-c** by cyclocondensation and the simultaneous deprotection of the benzoyl group. **4a-c** were coupled with the phenyl- or 4-chlorophenyl isothiocyanates to yield triazole-urea hybrids **11 g-l**. The remaining urea-azole conjugates were synthesized via Route-A, where the amine function was converted to the urea group in the first step. Compounds **5a-b** containing the ester structure was heated with hydrazine hydrate to obtain the corresponding hydrazide derivatives **6a-b**. These hydrazides directly gave the pyrazoles **8a-b** on reflux conditions with 2,4-dioxopentane in ethanol. The synthesis of oxadiazoles **9a-f** was started from hydrazides **6a-b** and it was observed that the hydrazides were converted to the corresponding thiosemicarbazides with the selected isothiocyanates in DMSO at room temperature. Since the conversion reaction with $KHSO_4$ to 1,3,4-oxadiazoles was also considered to be carried out in DMSO, both sequential reactions were carried out in one-pot at room temperature without isolating the thiosemicarbazides **7a-f**. However, thiosemicarbazides **7a-f** were obtained by the reaction of the hydrazides **6a-b** with methyl, ethyl or propyl isothiocyanates in ethanolic medium. The key intermediates **7a-f** were subjected to cyclocondensation reactions with H_2SO_4 and NaOH to give the 1,3,4-thiadiazoles **10a-f** and 1,2,4-triazoles **11a-f**, respectively. It was observed that the urea group present in compounds **7a-f** was stable and retained during these ring closing reactions.

Purity of the synthesized compounds was checked with TLC and HPLC. The structure of target azole-urea conjugates **8a-b, 9a-f, 10a-f** and **11a-l** were characterized by FTIR, ^{1}H NMR and ^{13}C NMR. All synthesized compounds were also characterized by LC-MS spectral data to confirm correct molecular ion peaks corresponding to $(M+H)^+$ in positive ionization and $(M\text{-}H)^-$ in negative ionization mode for each compound. In addition, to provide further support for the structures of target compounds, HMBC spectral findings were evaluated for compound **8a**.

It was observed that the -$NHNH_2$ protons of the hydrazides **6a-b** disappeared in the ^{1}H NMR spectra of the pyrazole derivatives **8a-b**, and methyl protons in the pyrazole ring appeared. C=O stretching vibrations detected at 1674–1639 cm^{-1} in hydrazide derivatives [20] shifted to 1667–1663 cm^{-1} in the FTIR spectra of pyrazole derivatives [21].

Thiosemicarbazide C=S stretching signals disappeared in the FTIR spectra of 1,3,4-oxadiazoles **9a-f** and 1,3,4-thiadiazoles **10a-f**, which were obtained from thiosemicarbazides **7a-f**. The chemical shift values of NH protons adjacent to heteroaromatic rings in **9a-f** and **10a-f** compounds were in the range of 7.73–7.48 ppm and 8.51–7.80 ppm, respectively [20]. Additionally, the C3 and C5 signals of oxadiazole and thiadiazole rings were observed in the expected regions in the ^{13}C NMR spectra, proving that rings were formed.

The N–H stretching bands of the triazole compounds **4a-c** and **11a-l** at 3364–3111 cm^{-1} were consistent with the literature [22]. 1,2,4-Triazole-3-thiones might have also existed in thiol form due to the tautomerization. Compounds containing 1,3,4-triazole moiety showed C=S stretching bands at 1277–1219 cm^{-1}. These values indicated that these rings exist in thione form, rather than thiol form [23]. The absence of S-H stretching bands in the region 2600–2550 cm^{-1} is another evidence of formation of the thione form [24]. ^{1}H NMR data of these compounds also supported the occurrence of thione form and the N–H protons of 1,2,4-triazole-3-thione were observed at 14.01–13.86 ppm whereas S-H proton was not detected [25]. In ^{13}C NMR spectra of triazoles **4a-c** and **11a-l,** C5 carbon of the triazole ring appeared at 151.80–150.89 ppm while the thiocarbonyl carbon was detected at 167.75–162.76 ppm in accordance with the literature [26].

HMBC analysis was applied to elucidate the carbon skeleton of compound **8a**, one of our pyrazole derivatives, and thus the structure was determined using ^{13}C-^{1}H interactions at two, three or more bond distances (Fig. 3). The interactions of the carbonyl group (C7) with the H2, H3, H5, H6 protons on the 1,4-disubstituted benzene ring confirmed that this carbon resonated at 166.44 ppm. Also, the peak observed at 152.76 ppm was attributed to the carbonyl of the urea (C19) due to its contour with the NH protons of urea around 8.80 and 9.00 ppm. The peak observed at 144.73 ppm was attributed to the C5 carbon of the pyrazole ring (C17) due to its contour with the H18 protons around 2.58 ppm, whereas the peak at 151.56 ppm was attributed to the C3 carbon of the pyrazole ring (C14) due to its interactions with H15 protons. Additionally, the C4 carbon atom of the pyrazole ring (C16) was detected at 111.34 ppm due to its interaction with the methyl protons of 3,5-dimethyl substitution. The methyl carbons of the 3,5-dimethylpyrazole ring were detected at 14.29 and 13.97 ppm, respectively with two symmetrical contours due to the interaction of own protons.

In this study, structural characterization of two new pyrazoles, six 1,3,4-oxadiazoles, four 1,3,4-thiadiazoles and ten 1,2,4-triazole-3-thione derivatives was carried out. However, despite all attempts, it was not possible to isolate compounds **10a, 10b, 11b** and **11e** in pure state during the post-synthetic work-up procedures. Consequently, all the new compounds except the four above-mentioned compounds were evaluated for their biological effects.

2.2. Biological evaluation

2.2.1. Screening of compounds against VEGFR-2

Newly synthesized compounds and positive controls, sorafenib and staurosporine were screened at 10 μM concentration on the activity of VEGFR-2 by ^{33}PanQinase™ assay performed by Reaction Biology Europe GMBH (and results were given in Table 1. The initial screening assay indicates that compound 1,3,4-thiadiazole derivative **10c**, pyrazole derivative **8a**, and 1,2,4-triazole derivative 11 g demonstrate the highest inhibitory activity with 11.5%, 22.5% and 30% residual

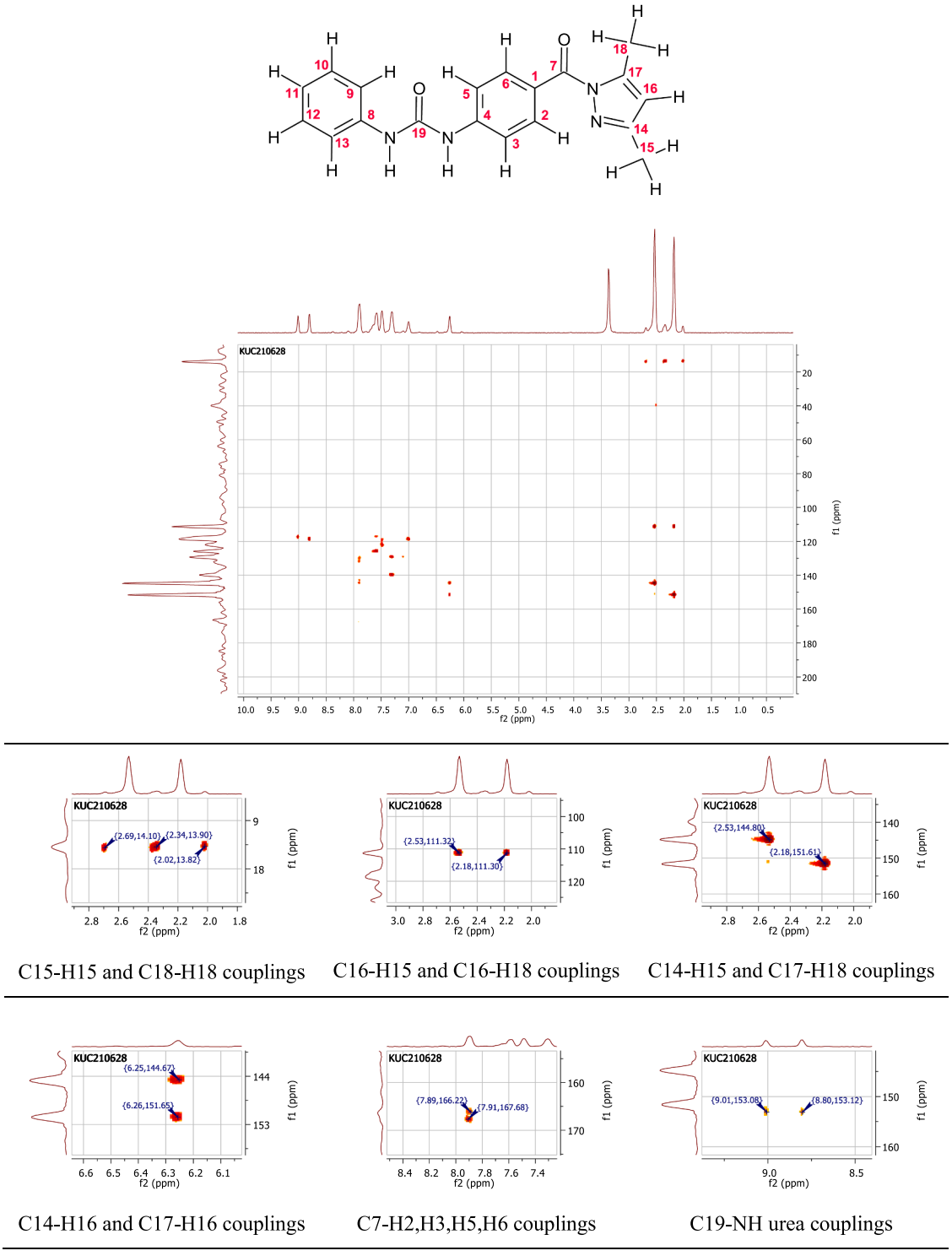

Fig. 3. HMBC spectrum of compound **8a**.

activities at 10 μM concentration, respectively. Compounds **11l** and 11 h also showed a moderate activity with less than 50% residual activity.

The diarylurea scaffold, due to its capacity to form H-bond interactions with various enzymes and receptors, is a privileged linker to combine various heterocyclic pharmacophoric components to design targeted and potent receptor tyrosine kinase inhibitors [27]. The electronic effect of the substituents on the phenyl ring is responsible for the inhibitory activity and cytotoxicity of these derivatives [28]. Among the pyrazole derivatives (**8a-b**) the addition of an electron withdrawing chlorine group to the phenyl ring (**8b**) drastically reduces the VEGFR-2 inhibitory activity. Similar results were observed for the 1,3,4-oxadiazole series (**9a-f**) although these derivatives were the least active VEGFR-2 inhibitors amongst all the studied compounds. The addition of *N*-methyl, *N*-ethyl or *N*-propyl substituent to the 1,3,4-oxadiazole does not change the inhibitory activity in a statistically significant way. When the activity of 1,3,4-thiadiazoles (**10c-f**) derivatives on VEGFR-2 activity examined, compound **10c** emerged as the most potent inhibitor amongst the tested compounds with only 11.5% residual activity at 10 μM concentration. Similar to pyrazole derivatives, addition of a chlorine group drastically reduces the VEGFR-2 inhibitory activity (75% residual

Table 1
The inhibitory activity of the synthesized compounds and positive controls sorafenib and staurosporine against VEGFR-2 and *in vitro* cytotoxicity against MCF-7, MDA-MB-231 and L-929 cell lines.

Compound	VEGFR-2 Residual activity (%) at 10 μM	VEGFR-2 IC_{50} (μM)	MCF-7 cell line IC_{50} (μM)	MDA-MB-231 cell line IC_{50} (μM)	L-929 Cell line IC_{50} (μM)
8a	**22.5 ± 3.536**	**1.154 ± 0.352**	**1.963 ± 0.19**	**3.48 ± 0.91**	**110.2 ± 2.52**
8b	83.0 ± 7.071	ND	79.57 ± 1.43	19.93 ± 1.16	177.5 ± 1.34
9a	92.0 ± 4.243	ND	18.91 ± 0.93	9.74 ± 1.18	153.6 ± 2.36
9b	86.5 ± 0.707	ND	25.81 ± 1.96	16.68 ± 1.71	102.8 ± 1.4
9c	89.0 ± 5.657	ND	54.65 ± 1.37	8.02 ± 1.08	131 ± 1.86
9d	87.5 ± 3.536	ND	**9.37 ± 0.66**	**5.83 ± 0.91**	**155.5 ± 2.38**
9e	97.0 ± 5.657	ND	46.8 ± 2.17	45.37 ± 2.02	117.6 ± 2.43
9f	97.0 ± 5.657	ND	46.8 ± 2.17	45.37 ± 2.02	117.6 ± 2.43
10c	**11.5 ± 2.121**	**0.664 ± 0.143**	40.11 ± 0.95	151.72 ± 2.49	63.87 ± 2.36
10d	74.0 ± 2.828	ND	15.69 ± 0.76	15.45 ± 1.34	28.4 ± 1.02
10e	50.5 ± 0.707	ND	34.11 ± 1.15	7.87 ± 1.19	67.71 ± 1.44
10f	75.5 ± 12.021	ND	48.11 ± 2.01	23.33 ± 1.99	136.8 ± 2.42
11a	52.0 ± 5.657	ND	26.31 ± 1.09	168.9 ± 2.55	155.7 ± 1.84
11c	75.5 ± 4.950	ND	27.33 ± 1.12	34.63 ± 1.87	78.52 ± 2.28
11d	70.5 ± 12.021	ND	122.6 ± 1.71	31.53 ± 2.18	64.69 ± 2.14
11f	77.0 ± 1.414	ND	78.54 ± 1.33	73.20 ± 2.72	37.79 ± 1.01
11 g	**30.0 ± 1.414**	**2.531 ± 1.009**	21.13 ± 0.90	20.73 ± 1.48	43.02 ± 0.93
11h	33.5 ± 3.536	ND	84.50 ± 1.45	166.1 ± 2.56	1.15 ± 0.3
11i	65.5 ± 7.708	ND	14.6 ± 0.99	55.39 ± 2.35	5.81 ± 1.49
11j	89.5 ± 4.950	ND	47.09 ± 1.25	31.19 ± 1.95	75.54 ± 2.75
11k	68.5 ± 7.778	ND	24.84 ± 0.70	6.71 ± 0.99	9.81 ± 0.34
11l	44.5 ± 2.121	ND	9.187 ± 0.58	1.96 ± 0.02	4.75 ± 0.36
Sorafenib	0.5 ± 0.707	0,089 ± 0.008	15.09 ± 1.05	5.29 ± 0.82	29.36 ± 1.08
Staurosporine	0.5 ± 0.707	ND	ND	ND	ND

ND: Not determined.
All results were given as the mean ± SD of three independent experiments $P< 0.5$, two-tailed Student's t-test.

activity for the corresponding chlorinated compound **10f**). Finally, for the 1,2,4-triazole-3-thione derivatives addition of triflouromethyl group on the 3- position of the phenyl increases the inhibitory potential of the derivatives when compared to addition on the 4- position, while addition of a chlorine substituent decrease the inhibitory activity.

2.2.2. *Determination of the IC_{50} values of the most active compounds*

The three most potent inhibitors of VEGFR-2-catalyzed phosphorylation activity determined in the screening assay were further analyzed by a dose-response assay at five different concentrations in the range of 10–10 μM using the well-established FRET-based Z′-Lyte assay (see Suppl. Materials). The results were given in Table 1. Compound **10c**, 1-phenyl-3-[4-[5-(*propylamino*)−1,3,4-*thiadiazol*-2-*yl*]phenyl]urea, was found to be the most potent inhibitor of VEGFR-2 mediated phosphorylation activity with an IC_{50} value of 0.664 μM, followed by **8a** and 11 g with IC_{50} values of 1.154 μM and 2.531 μM, respectively. The positive control sorafenib outperformed all other examined compounds in the same assay in terms of its inhibitory effect, with an IC_{50} value of 0.089 μM. Compound **10c**, however, exhibits comparable inhibitory action.

2.2.3. *In vitro anti-proliferative activity against normal and cancer cells*

According to Table 1 compounds **8a** and **9d** showed the highest cytotoxic activity against MCF-7 human breast carcinoma (IC_{50} = 1.963 μM and 9.37 μM, respectively) and MDA-MB-231 triple-negative human breast adenocarcinoma cell lines (IC_{50} = 3.48 μM and 5.83 μM, respectively). In order to compare the cytotoxic activity over normal cells and determine their selectivity, non-cancerous fibroblast cells (L929) also used in the MTT assay, and compounds **8a** and **9d** showed much lower toxicity against this cell line with IC_{50} values of 110.2 μM and 155.5 μM, respectively. **8a** demonstrated 56-fold more activity towards MCF-7 and 32-fold more activity towards MDA-MB-231 cell lines when compared to L929 fibroblast cells. **8a** displayed more cytotoxic activity when compared with sorafenib against MCF-7 and MDA-MB-231 cell lines while displaying 3.8-fold less toxicity against the normal L929 cell line.

Among the pyrazole derivatives (**8a-b**), compound **8a** (R_1 = H) displayed considerably higher antiproliferative activity against MCF-7 and MDA-MB-231 cell lines when compared to its chlorinated derivative **8b** (R_1= Cl). For the 1,3,4-oxadiazole series (**9a-f**) all compounds displayed higher cytotoxicity against MDA-MB-231 cell lines and lower toxicity against the normal L929 cell line. Compound **9d** (R_1= 4-Cl, R_2= Me) is the most potent compound in this series in terms of its cytotoxicity against MCF-7 and MDA-MB-231 cell lines and performed significantly better when compared to its ethyl and propyl derivatives, compound **9e** and **9f**, respectively. 1,3,4-thiadiazole derivatives (**10a-f**) displayed moderate antiproliferative activities against the tested cell lines, and compound **10f** (R_1=Cl, R_2= Pr) revealed as the most active compound in this series. Lastly, for the 1,2,4-triazole-3-thione derivatives (**11a-l**) it was found that the addition of the trifluoromethyl group (**11 g-l**) greatly improved their cytotoxicity against all tested cell lines.

2.2.4. *Annexin-V/PI assay with flow cytometry*

An important marker for the detection of apoptosis in cells is annexin-V/PI binding. Annexin V binds to phosphatidylserine in the cell membrane and binds to nucleic acids when the PI core structure is disrupted. Only Annexin-V binding was seen in the early stages of apoptosis and both Annexin-V and PI binding were seen in the late stages of apoptosis. Compared to the control, compounds **9d** and **8a** significantly increased early and late apoptosis in MCF-7 cells (Fig. 4). In MDA-MB-231 cells, compounds **9d** and **8a** was not significantly change early apoptosis but increased late apoptosis and necrosis (Fig. 4).

2.3. *In silico studies*

2.3.1. *Molecular docking*

The crystal structure of vascular endothelial growth factor receptor-2 (VEGFR-2) protein complexed with the angiogenesis inhibitor Sorafenib (PDB ID: 4ASD; resolution: 2.03 Å) was retrieved from the Protein Data Bank and after the optimizations were done AutoDock4 docking program employed for docking of ligands. The result of each docked molecule was determined according to the affinity energy (kcal/mol) of the receptor-ligand complex (Table 2). The best conformation structures were saved, and resultant ligand receptor complexes' visualization was rendered as 2D and 3D pictures in Fig. 4.

The detailed interactions of the docked poses of the two best

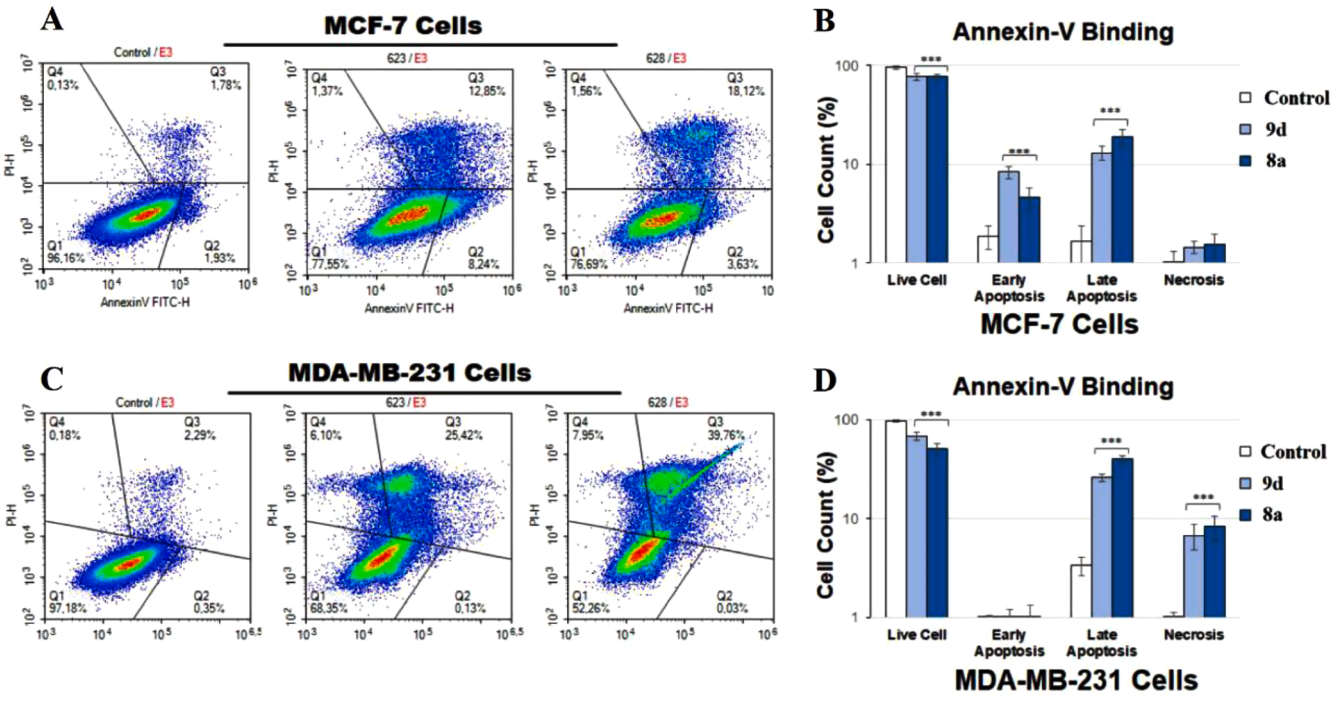

Fig. 4. Annexin-V/PI binding levels of compound 9d and 8a treatment to MCF-7 and MDA-MB-231 cells (a-c) Flowcytometry binding images of compound, (b-d) Cell count of early and late apoptotic cells and necrotic cells (***p <0.001 compare to control cells).

Table 2
Gibbs free energy of binding, calculated inhibition constants for the synthesized compounds and controls sorafenib and staurosporine.

Compound	Lowest Binding Energy (ΔG, kcal/mol)	K_i[a] (μM)
8a	-9.0	0.264
8b	-9.6	0.208
9a	-9.1	0.254
9b	-9.0	0.264
9c	-9.0	0.264
9d	-9.5	0.216
9e	-9.3	0.234
9f	-9.3	0.234
10c	-9.0	0.264
10d	-9.3	0.234
10e	-9.2	0.243
10f	-9.3	0.234
11a	-8.8	0.287
11c	-8.9	0.275
11d	-8.9	0.275
11f	-8.0	0.396
11g	-9.5	0.216
11h	-9.9	0.184
11i	-9.6	0.208
11j	-10.0	0.177
11k	-9.9	0.184
11l	-9.9	0.184
Sorafenib	-10.2	0.163
Staurosporine	-8.1	0.380

[a] $K_i = \exp[(\Delta G \times 1000) / (R \times T)$.

inhibiting compounds (**10c** and **8a**) and sorafenib were selected to render visible. Analysis of the optimal binding mode for sorafenib (Fig. 5) in the VEGFR-2 binding site cavity revealed that sorafenib is surrounded by various side chain residues seen in 2D and 3D pictures making electrostatic and van der Waals interactions with binding site residues lining the cavity. Conventional hydrogen bonds occur between the amide group of sorafenib and GLU885 and ASP1046. The other electrostatic solid interactions occur between CYS1045, CYS915 residues, and the sorafenib. The other interacting amino acid residues with sorafenib are PHE1047, PHE918, ILE1044, and ALA868. Fig. 5 shows the 2D and 3D pictures of compound **10c** in the binding site of the receptor. Analysis of the optimal binding mode for compound **10c** in the VEGFR-2 binding site cavity revealed that one favorable conventional hydrogen bond occurs between ASP1046 and the urea-NH moiety of compound **10c**. LEU889 and ALA886 residues make two very effective pi-sigma attractions with the inhibitors. The residue CYC1045 forms pi-sulfur interaction with the benzene ring of the inhibitor. The other various van der Waals and pi-alkyl interactions make this compound a very potent inhibitor against the VEGFR-2 receptor. Fig. 5 indicates the poses (2D on the left, 3D on the right) of compound **8a** in the receptor's binding site. The residue ASP1046 makes one strong conventional hydrogen bond with the urea-NH group of compound **8a**. The CYS1045 makes a pi-sulfur bond with the phenyl ring of compound **8a**. LEU889 side chain of the receptor makes a pi-sigma attraction with the inhibitor. The other van der Waals and electrostatic interactions occurring between the inhibitor and the residues lining the binding sites of the receptor effectively increase the potency of **8a** against the VEGFR-2 receptor.

2.3.2. In silico prediction of physico-chemical and pharmacokinetic properties

Pharmacokinetic and physicochemical properties of the synthesized compounds and control compounds sorafenib and staurosporine was investigated using SwissADME website (http://www.swissadme.ch/index.php) and results were given in Table 3. A model for lipophilicty prediction, the WLOGP vs. TPSA (topological polar surface area) BOILED-Egg graph for the compounds presented is shown in Fig. 6 [29]. Fig. 7 shows the bioavailability radar, which is a plot of six different physicochemical properties, including size, polarity, lipophilicity, solubility, flexibility, and saturation [30].

Based on these data, all tested compounds satisfy the "Rule of Five" proposed by Lipinski [31] and except compounds **11g-l**, displayed characteristics that were comparable or better to those of sorafenib. Oral bioavailability is frequently a crucial factor in the development of bioactive compounds as drug candidates. All tested compounds

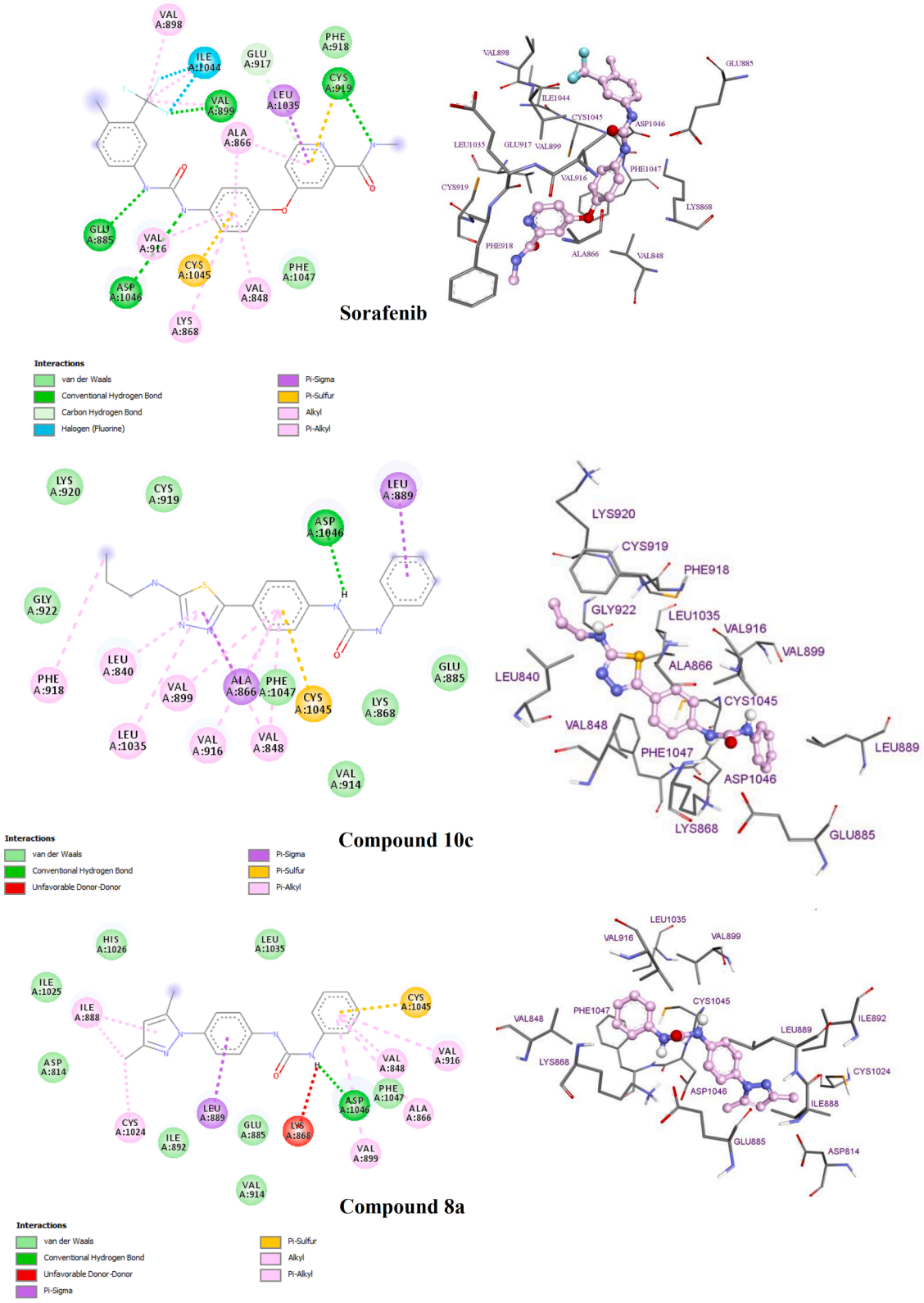

Fig. 5. Two-dimensional (left) and three-dimensional (right) pictures of sorafenib, **10c** or **8a** in the active site of the VEGFR-2 protein were shown. Amino acid side chains are shown as sticks; the inhibitor is shown as a ball and stick (pink). In the 2D picture, the interaction designations were given as an insert.

predicted to have high intestinal absorption and, except **9a-b**, with no Blood Brain Barrier permeability. Rotatable bound (RB) number is another descriptor of oral bioavailability [32], and all tested compounds were predicted to have lower number of RBs when compared to sorafenib.

3. Conclusion

In the present work, according to our hybridization plan between an FDA-approved VEGFR-2 inhibitor, sorafenib, two new pyrazoles, six 1,3,4-oxadiazoles, four 1,3,4-thiadiazoles, and ten 1,2,4-triazole-3-

Table 3
Predicted pharmacokinetics and physicochemical properties of synthesized compounds as compared to sorafenib.

Cmpd	MW	Fraction Csp3	RB	HBA	HBD	MR	TPSA	Log P	GI absoption	BBB perm.	Lip. V.	Bio. *Sc.*
10c	353.44	0.17	8	3	3	102.99	107.18	3.43	High	No	0	0.55
10d	359.83	0.06	6	3	3	98.38	107.18	3.26	High	No	0	0.55
10e	373.86	0.12	7	3	3	103.19	107.18	3.61	High	No	0	0.55
10f	387.89	0.17	8	3	3	108	107.18	3.95	High	No	0	0.55
11a	325.39	0.06	5	2	3	92.83	106.83	2.67	High	No	0	0.55
11c	353.44	0.17	7	2	3	102.45	106.83	3.25	High	No	0	0.55
11d	359.83	0.06	5	2	3	97.84	106.83	3.21	High	No	0	0.55
11f	387.89	0.17	7	2	3	107.46	106.83	3.75	High	No	0	0.55
11g	393.39	0.12	6	5	3	97.83	106.83	3.75	Low	No	0	0.55
11h	407.41	0.17	7	5	3	102.64	106.83	3.93	Low	No	0	0.55
11i	421.44	0.21	8	5	3	107.45	106.83	4.27	Low	No	0	0.55
11j	393.39	0.12	6	5	3	97.83	106.83	3.72	Low	No	0	0.55
11k	407.41	0.17	7	5	3	102.64	106.83	3.96	Low	No	0	0.55
11l	421.44	0.21	8	5	3	107.45	106.83	4.28	Low	No	0	0.55
8a	306.36	0.11	5	2	2	92.22	58.95	3.07	High	Yes	0	0.55
8b	340.81	0.11	5	2	2	97.23	58.95	3.59	High	Yes	0	0.55
9a	309.32	0.06	6	4	3	87.76	92.08	2.26	High	No	0	0.55
9b	323.35	0.12	7	4	3	92.57	92.08	2.59	High	No	0	0.55
9c	337.38	0.17	8	4	3	97.38	92.08	2.96	High	No	0	0.55
9d	343.77	0.06	6	4	3	92.77	92.08	2.8	High	No	0	0.55
9e	357.79	0.12	7	4	3	97.58	92.08	3.14	High	No	0	0.55
9f	371.82	0.17	8	4	3	102.39	92.08	3.51	High	No	0	0.55
S	464.82	0.1	9	7	3	112.48	92.35	4.1	Low	No	0	0.55
St	482.53	0.32	2	7	5	142.88	103.88	1.98	High	No	0	0.55

S: Sorafenib; St: Staurosporine; BBB perm.: BBB permeability; Lip. V.: Lipinski violation; Bio. *Sc.*: Bioavailability Score.

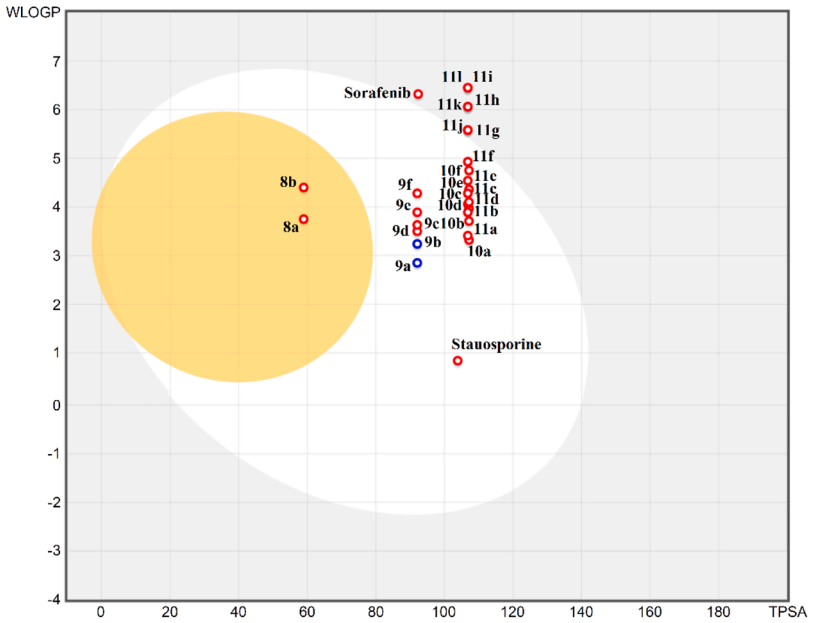

Fig. 6. Predicted Boiled-Egg plot from SwissADME online web tool for compounds **8a-b, 9a-f, 10a-f**, and **11a-l** and controls staurosphorine and sorafenib.

thione derivatives bearing urea moieties were synthesized and characterized according to their spectral data. Preliminary screening of our 22 newly synthesized compounds and positive controls (sorafenib and staurosporin) at one concentration (10 μM) on the activity of VEGFR-2 was performed by Reaction Biology Europe (RBE) GMHB (Freiburg, Germany) using a ^{33}PanQinase™ assay. Seven of the compounds, namely **8a, 10c, 10e, 11a**, 11 g, 11 h and **11l**, displayed moderate to high inhibitory activity against VEGFR-2. Among them, the most potent derivatives with% VEGFR-2 residual activities lower than 30%, **10c, 8a**, and 11 g, were selected for further dose-dependent inhibition studies at five different concentrations in the range of 10–10 μM using the well-established FRET-based Z′-Lyte assay and IC_{50} values were calculated as 0.664 μM, 1.154 μM and 2.531 μM, respectively. *In vitro* anti-proliferative activity of the synthesized compounds against breast carcinoma (MCF-7) cell line, triple negative human breast adenocarcinoma (MDA-MB-231) cell line and non-cancerous fibroblast cells (L929) was performed utilizing the MTT assay. Compounds **8a, 9d**, and **11l** displayed superior anti-proliferative activity against MCF-7 and MDA-MB-231 cell lines when compared to sorafenib. Furthermore, compounds **8a** and **9d** showed lower cytotoxicity than sorafenib on non-cancerous L929 cell line. Annexin-V/PI binding assay for compound **8a** and **9d** was performed by using flow cytometry and it was revealed that they significantly increased early and late apoptosis in MCF-7 cells and late apoptosis and necrosis in MDA-MB-231 cells. To explain the anti-VEGFR-2 activity of the synthesized compounds, docking studies were done at the VEGFR-2 active site. *In silico* ADME predictions, showed that most of our tested compounds including **8a** show favorable pharmacokinetic characteristics when compared to sorafenib. According

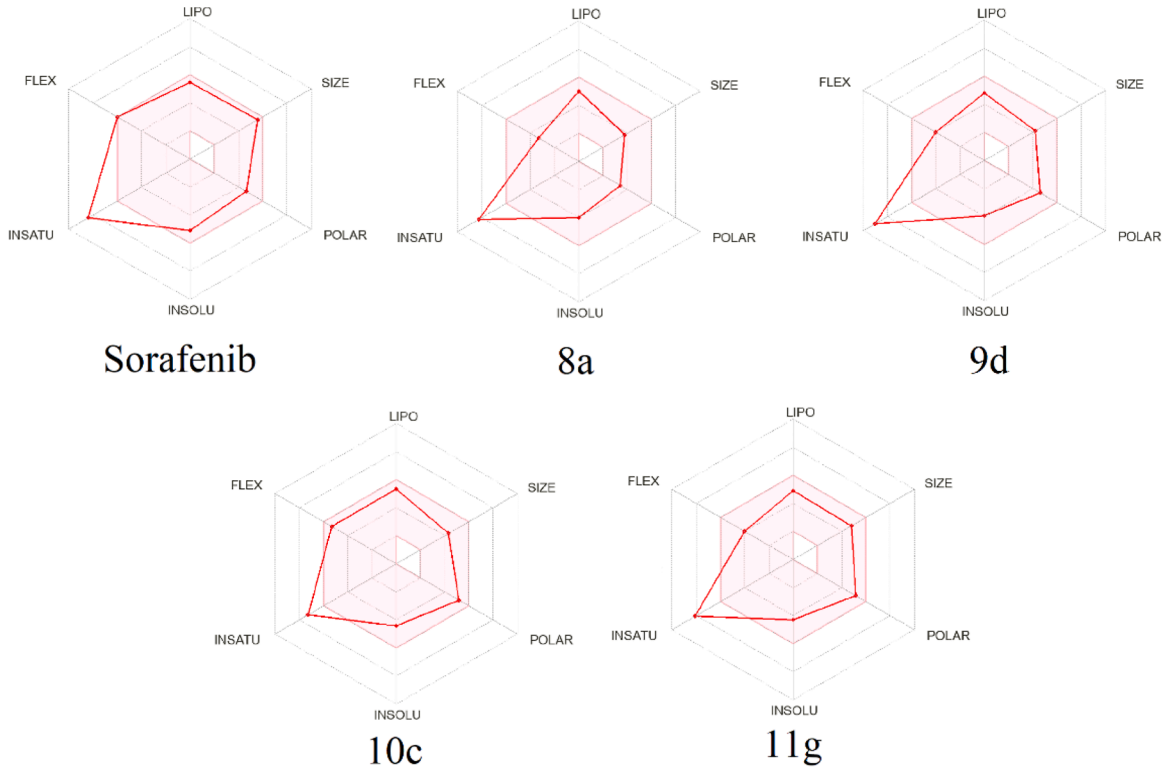

Fig. 7. Bioavailability radar charts from *SwissADME* online web tool for compounds **8a, 9d, 10c** and **11f** and control sorafenib.

to these results, pyrazole derivative **8a** emerged as a promising inhibitor of VEGFR-2 activity with selective and potent cytotoxicity against MCF-7 and MDA-MB-231 cells.

4. Experimental

4.1. Chemistry

All melting points obtained by the open capillary method on a Schmelzpunktbestimmer SMP II melting point apparatus were uncorrected. Infrared spectra recorded on a Shimadzu FTIR-8400S spectrophotometer, and ^{1}H NMR and ^{13}C NMR spectra were recorded on a Brüker 400 MHZ-NMR spectrophotometer. Chemical shifts expressed in values (ppm) using TMS are used as an internal standard in deuterated DMSO. The abbreviations used are as follows: s, singlet; d, doublet; m, multiplet. TLC monitored the progress of the reaction and used a UV lamp as an indicator. Mass spectra were measured on the mass spectra were recorded on Shimadzu LC-MS/MS-8030 system (Shimadzu Corporation, Kyoto, Japan). The instrument was operated using positive electrospray ionization (ESI) mode.

The synthetic procedures and analytical findings of compounds **1, 2, 3a-c, 4a-c, 5a-b, 6a-b** and **7a-f** which are intermediates used in the synthesis of target compounds, are presented in the supplementary material file.

4.1.1. General procedure for the synthesis of target compounds 8a-b

A mixture of **6a–b** (2 mmol) and 2,4-dioxopentane (2 mmol) in 10 ml of absolute ethanol was refluxed for 4 h. Then, the reaction mixture was cooled and poured onto water, and the precipitated product was filtered, dried, and crystallized from ethanol.

4.1.1.1. 1-{4-[(3,5-Dimethyl-1H-pyrazol-1-yl)carbonyl]phenyl}−3-phenylurea 8a. White solid; yield 38%; HPLC t_R (min): 7.69; m.p. 222–224 °C; FTIR (cm^{-1}): 3283 (N—H str), 1697, 1667 (C=O). ^{1}HNMR Spectrum δ ppm (300 MHz, DMSO d_6): 9.00 and 8.80 (s, 2H, urea N*H*); 7.89 (d, 4H, *J* = 8.5 Hz, Ar*H*); 7.47 (d, 2H, *J* = 8.4 Hz, Ar*H*); 7.30 (t, 2H, *J* = 7.9 Hz, Ar*H*); 7.00 (t, 1H, *J* = 7.4 Hz, Ar*H*); 6.25 (s, 1H, pyrazole C*H*); 2.58 (s, 3H, pyrazole C5-C*H*$_3$); 2.18 (s, 3H, pyrazole C3-C*H*$_3$). ^{13}CNMR Spectrum δ ppm (75 MHz, DMSO d_6): 166.44 (pyrazole-*C* = O); 152.76 (urea *C* = O); 151.56 (pyrazole *C3*); 144.73 (pyrazole *C5*); 143.56, 139.87, 133.08, 129.31, 126.05, 122.60, 118.84, 117,60 (Ar*C*); 111.34 (pyrazole *C4*) 14.29 (pyrazole C3-*C*H$_3$); 13.97 (pyrazole C5-*C*H$_3$). LR-MS (ESI) (*m/z*): calculated [M + Na]$^+$: 357.13, found: 357.20; calculated for [M - H]$^-$: 333.14, found: 333.20.

1-(4-chlorophenyl)−3-{4-[(3,5-*dimethyl*-1H-*pyrazol*-1-*yl*)*carbonyl*] phenyl}urea **8b:** White solid; yield 73%; HPLC t_R (min): 4.84; m.p. 211–212 °C; FTIR (cm^{-1}): 3536, 3337 (N—H str), 1697, 1663 (C=O). ^{1}HNMR Spectrum δ ppm (400 MHz, DMSO d_6): 9.17 and 8.99 (s, 2H, urea N*H*); 7.91 (d, 2H, *J* = *8.8 Hz*, Ar*H*); 7.55 (dd, 4H, *J* = *8.8 Hz*, Ar*H*); 7.36 (d, 2H, *J* = *9.2 Hz*, Ar*H*); 6.27 (s,1H, pyrazole C*H*); 2.54–2.51 (m, 3H, DMSO and pyrazole C5-C*H*$_3$); 2.19 (s, 3H, pyrazole C3-C*H*$_3$). ^{13}CNMR Spectrum δ ppm (100 MHz, DMSO d_6): 167.33 (pyrazole-*C*=O); 152.59 (urea *C*=O); 151.60 (pyrazole *C3*); 144.75 (pyrazole *C5*); 144.25, 138.78, 133.20, 129.16, 126.24, 126.14, 120.42, 117,16 (Ar*C*); 111.37 (pyrazole *C4*) 14.30 (pyrazole C3-*C*H$_3$); 13.96 (pyrazole C5-*C*H$_3$). LR-MS (ESI) (*m/z*): calculated [M + Na]$^+$: 391.09, found: 391.15; calculated [M + H]$^+$: 369.11, found: 369.20; calculated for [M - H]$^-$: 367.10, found: 367.15.

4.1.2. General procedure for the synthesis of target compounds 9a–f

A solution of compounds **6a–b** (1.5 mmol) and isothiocyanate derivatives (1.5 mmol) in DMSO (5 mL) was stirred at room temperature for 3 h. Then, $KHSO_4$ (7.5 mmol) was directly added to the stirred solution at room temperature and reacted for another 8 h. After the completion of the reaction monitored by TLC, the solution was diluted with 30 mL of water, and the resulting precipitate was filtered, dried, and crystalised with ethanol.

4.1.2.1. 1-(4-(5-(Methylamino)−1,3,4-oxadiazol-2-yl)phenyl)−3-phenylurea 9a. Brown solid; yield 45%, HPLC t_R (min): 5.27; m.p. 279–281 °C; FTIR (cm^{-1}): 3273, 3123 (N—H str), 1687 (C=O). ^{1}HNMR Spectrum δ ppm (400 MHz, DMSO d_6): 9.13 and 8.90 (s, 2H, urea N*H*); 7.87 (d, 2H,

J = *8.8 Hz*, Ar*H*); 7.76 (d, 2H, *J* = *8.8 Hz*, Ar*H*); 7.69 (s, 1H, N*H*—CH_3); 7.61 (d, 2H, *J* = *7.6 Hz*, Ar*H*); 7.44 (d, 2H, *J* = *8.0 Hz*, Ar*H*); 7.14 (t, 1H, *J* = *7.2 Hz*, Ar*H*); 2.95 (d, 3H, *J* = *4.8 Hz*, NH—*C*H_3). ^{13}CNMR Spectrum δ ppm (100 MHz, DMSO d_6): 164.31 (oxadiazole *C5*); 158.15 (oxadiazole *C3*); 152.74 (urea *C*=O); 142.25, 139.87, 129.29, 126.54, 122.56, 118.81, 118.66, 118.00 (Ar*C*); 29.52 (NH—*C*H_3). LR-MS (ESI) (*m/z*): calculated $[M + H]^+$: 310.13, found: 310.30; calculated for $[M - H]^-$: 308.12, found: 308.25.

4.1.2.2. 1-(4-(5-(Ethylamino)−1,3,4-oxadiazol-2-yl)phenyl)−3-phenylurea 9b. Orange solid; HPLC t_R (min): 6.35; yield 38%, m.p. 288–290 °C; FTIR (cm^{-1}): 3276 (N—H str), 1693 (C=O). ^{1}HNMR Spectrum δ ppm (400 MHz, DMSO d_6): 9.00 and 8.77 (s, 2H, urea N*H*); 7.73 (d, 2H, *J* = *7.2 Hz*, Ar*H*); 7.67 (s, 1H, N*H*—CH_3); 7.61 (d, 2H, *J* = *8.8 Hz*, Ar*H*); 7.47 (d, 2H, *J* = *8.4 Hz*, Ar*H*); 7.30 (t, 2H, *J* = *7.2 Hz*, Ar*H*); 7.00 (t, 1H, Ar*H*); 3.48–3.25 (m, 2H, DMSO and NH—C*H*$_2$—CH_3); 1.19 (t, 3H, *J* = *7.2 Hz*, NH—C*H*$_3$). ^{13}CNMR Spectrum δ ppm (100 MHz, DMSO d_6): 163.60 (oxadiazole *C5*); 157.99 (oxadiazole *C3*); 152.77 (urea *C*=O); 142.23, 139.88, 129.29, 126.52, 122.56, 118.80, 118.67, 118.02 (Ar*C*); 37.90 (NH—CH_2—CH_3); 15.02 ($NHCH_2$—*C*H_3). LR-MS (ESI) (*m/z*): calculated $[M + H]^+$: 324.15, found: 324.35; calculated for $[M - H]^-$: 322.13, found: 322.30.

4.1.2.3. 1-Phenyl-3-(4-(5-(propylamino)−1,3,4-oxadiazol-2-yl)phenyl) urea 9c. Light brown solid; yield 43%, HPLC t_R (min): 7.27; m.p. 288–290 °C; FTIR (cm^{-1}): 3277 (N—H str), 1687 (C=O). ^{1}HNMR Spectrum δ ppm (400 MHz, DMSO d_6): 9.00 and 8.99 (s, 2H, urea N*H*); 7.73–7.60 (m, 5H, N*H*—CH_3 and Ar*H*); 7.46 (d, 2H, *J* = *7.6 Hz*, Ar*H*); 7.30 (d, 2H, *J* = *6.8 Hz*, Ar*H*); 7.00 (t, 1H, *J* = *6.8 Hz*, Ar*H*); 3.20 (t, 2H, *J* = *6.8 Hz*, NH—C*H*$_2$—C_2H_5); 1.63–1.58 (m, 2H, $NHCH_2$—C*H*$_2$—CH_3); 0.94 (t, 3H, *J* = *6.0 Hz*, NHC_2H_4—*C*H_3). ^{13}CNMR Spectrum δ ppm (100 MHz, DMSO d_6): 163.77 (oxadiazole *C5*); 157.91 (oxadiazole *C3*); 152.74 (urea *C*=O); 142.21, 139.86, 129.29, 126.51, 122.58, 118.81, 118.68, 118.03 (Ar*C*); 44.83 (NH—*C*H_2—C_2H_5); 22.55 ($NHCH_2$—*C*H_2—CH_3); 11.71 (NHC_2H_4—*C*H_3). LR-MS (ESI) (*m/z*): calculated $[M + H]^+$: 338.16, found: 338.35; calculated for $[M - H]^-$: 336.15, found: 336.30.

4.1.2.4. 1-(4-Chlorophenyl)−3-(4-(5-(methylamino)−1,3,4-oxadiazol-2-yl)phenyl)urea 9d. White solid; yield 45%, HPLC t_R (min): 7.18; m.p. 290–292 °C; FTIR (cm^{-1}): 3354 (N—H str), 1697 (C=O). ^{1}HNMR Spectrum δ ppm (400 MHz, DMSO d_6): 9.04 and 8.91 (s, 2H, urea N*H*); 7.73 (d, 2H, *J* = *8.0 Hz*, Ar*H*); 7.61 (d, 2H, *J* = *8.4 Hz*, Ar*H*); 7.57 (s, 1H, N*H*—CH_3); 7.50 (d, 2H, *J* = *8.4 Hz*, Ar*H*); 7.35 (d, 2H, *J* = *8.8 Hz*, Ar*H*); 2.86 (d, 3H, *J* = *4.8 Hz*, NH—C*H*$_3$). ^{13}CNMR Spectrum δ ppm (100 MHz, DMSO d_6): 161.93 (oxadiazole *C5*); 157.28 (oxadiazole *C3*); 152.14 (urea *C*=O); 142.09, 138.44, 128.61, 126.26, 125.58, 119.84, 118.27, 116.93 (Ar*C*); 14.34 (NH—CH_3). LR-MS (ESI) (*m/z*): calculated for $[M - H]^-$: 342.08, found: 342.20.

4.1.2.5. 1-(4-Chlorophenyl)−3-(4-(5-(ethylamino)−1,3,4-oxadiazol-2-yl)phenyl)urea 9e. White solid; yield 52%; HPLC t_R (min): 9.00; m.p. 209–211 °C; FTIR (cm^{-1}): 3342, 3276 (N—H str), 1706 (C=O). ^{1}HNMR Spectrum δ ppm (400 MHz, DMSO d_6): 9.12 and 8.98 (s, 2H, urea N*H*); 8.12 (s, 1H, N*H*—CH_3); 7.74 (dd, 2H, *J* = *8.4 Hz*, Ar*H*); 7.61 (dd, 2H, *J* = *8.8 Hz*, Ar*H*); 7.51 (d, 2H, *J* = *8.8 Hz*, Ar*H*); 7.34 (d, 2H, *J* = *8.8 Hz*, Ar*H*); 4.00 (t, 2H, NH—C*H*$_2$—CH_3); 1.19 (t, 3H, *J* = *7.2 Hz*, NH—C*H*$_3$). ^{13}CNMR Spectrum δ ppm (100 MHz, DMSO d_6): 161.93 (oxadiazole *C5*); 157.28 (oxadiazole *C3*); 152.14 (urea *C*=O); 142.09, 138.44, 128.61, 126.26, 125,58, 119.84, 118.27, 116.93 (Ar*C*); 37.57 (NH—*C*H_2—CH_3); 14.34 ($NHCH_2$—*C*H_3). LR-MS (ESI) (*m/z*): calculated $[M + H]^+$: 358.11, found: 358.30; calculated for $[M - H]^-$: 356.09, found: 356.25.

4.1.2.6. 1-(4-Chlorophenyl)−3-(4-(5-(propylamino)−1,3,4-oxadiazol-2-yl)phenyl)urea 9f. White solid; yield 43%; HPLC t_R (min): 12.04; m.p. 234–236 °C; FTIR (cm^{-1}): 3273 (N—H str), 1703 (C=O). ^{1}HNMR Spectrum δ ppm (400 MHz, DMSO d_6): 9.18 and 9.06 (s, 2H, urea N*H*); 7.88–7.48 (m, 9H, N*H*—CH_3 and Ar*H*); 3.32 (t, 2H, *J* = *6.8 Hz*, NH—C*H*$_2$—C_2H_5); 1.76–1.71 (m, 2H, $NHCH_2$—*C*H_2—CH_3); 1.06 (t, 3H, *J* = *7.2 Hz*, NHC_2H_4—C*H*$_3$). ^{13}CNMR Spectrum δ ppm (100 MHz, DMSO d_6): 163.28 (oxadiazole *C5*); 157.38 (oxadiazole *C3*); 152.16 (urea *C*=O); 141.54, 138.42, 128.63, 126.00, 125.58, 119.84, 118.29, 117.70 (Ar*C*); 44.35 (NH—*C*H_2—C_2H_5); 22.06 ($NHCH_2$—*C*H_2—CH_3); 11.23 (NHC_2H_4—*C*H_3). LR-MS (ESI) (*m/z*): calculated $[M + H]^+$: 372.12, found: 372.30; calculated for $[M - H]^-$: 370.11, found: 370.25.

4.1.3. General procedure for the synthesis of target compounds 10a–f

About 1 mmol of thiosemicarbazide derivatives (**7a-f**) were added to 10 mL of sulfuric acid at 60 °C and stirred for 8 h. The reaction was monitored with TLC, at the end of the reaction, the mixture was poured into ice water. The precipitated solid was filtered off and washed with hot ethanol.

4.1.3.1. 1-{4-[5-(Propylamino)−1,3,4-thiadiazol-2-yl]phenyl}−3-phenylurea 10c. Yield 45%; HPLC t_R (min): 7.41; m.p. 196–198 °C; FTIR (cm^{-1}): 3354, 3273 (NH str.), 1699 (C=O). ^{1}HNMR Spectrum δ ppm (400 MHz, DMSO d_6): 8.99 and 8.80 (s, 2H, urea N*H*); 7.95 (s, 1H, N*H*—C_3H_7); 7.70 (dd, 4H, *J* = *8.4 Hz*, Ar*H*); 7.52 (d, 2H, *J* = *7.6 Hz*, Ar*H*); 7.35 (t, 2H, *J* = *7.6 Hz*, Ar*H*); 7.05 (t, 1H, *J* = *7.6 Hz*, Ar*H*); 3.98 (t, 2H, NH—C*H*$_2$—C_2H_5); 1.69–1.62 (m, 2H, $NHCH_2$—C*H*$_2$—CH_3); 0.92 (t, 3H, *J* = *7.2 Hz*, NHC_2H_4—C*H*$_3$). ^{13}CNMR Spectrum δ ppm (100 MHz, DMSO d_6): 168.44 (thiadiazole *C5*); 156.07 (thiadiazole *C3*); 152.80 (urea *C*=O); 141.61, 139.95, 129.29, 127.54, 124.73, 122.50, 118.79, 118.70 (Ar*C*); 47.14 (NH—C*H*$_2$—C_2H_5); 22.30 ($NHCH_2$—*C*H_2—CH_3); 11.87 (NHC_2H_4—*C*H_3). LR-MS (ESI) (*m/z*): calculated [M + H]+: 354.14, found: 354.10; calculated for [M - H]-: 352.12, found: 352.15.

4.1.3.2. 1-(4-Chlorophenyl)−3-{4-[5-(methylamino)−1,3,4-thiadiazol-2-yl]phenyl}urea 10d. Yield 80%; HPLC t_R (min): 6.28; m.p. 244 °C; FTIR (cm^{-1}): 3321, 3273 (NH str.), 1699 (C=O). ^{1}HNMR Spectrum δ ppm (400 MHz, DMSO d_6) 8.99 and 8.91 (s, 2H, N*H*, urea); 7.80–7.33 (m, 9H, Ar*H* and N*H*—CH_3); 2.93 (s, 3H, N—C*H*$_3$). ^{13}CNMR Spectrum δ ppm (100 MHz, DMSO d6): 169.17 (thiadiazole *C5*); 156.30 (thiadiazole *C2*); 152.70 (urea *C* = O); 141.38, 138.98, 129.13, 127.54, 126.02, 124.98, 120.32, 118.82 (Ar*C*); 31.76 (N—CH_3). LR-MS (ESI) (*m/z*): calculated [M + H]+: 360.07, found: 360.10; calculated for [M - H]-: 358.05, found: 358.10.

4.1.3.3. 1-(4-Chlorophenyl)−3-{4-[5-(ethylamino)−1,3,4-thiadiazol-2-yl]phenyl}urea 10e. Yield 86%; HPLC t_R (min): 12.57; m.p. 305–306 °C; FTIR (cm^{-1}): 3316, 3271 (NH str.), 1699 (C = O). ^{1}HNMR Spectrum δ ppm (400 MHz, DMSO d_6): 8.98 and 8.89 (s, 2H, N*H*, urea); 7.85 (s, 1H, -N*H*—CH_3); 7.68 (d, 2H, *J* = *6 Hz*, Ar*H*); 7.56 (d, 2H, *J* = *6 Hz*, Ar*H*); 7.51 (d, 2H, *J* = *6 Hz*, Ar*H*); 7.34 (d, 2H, *J* = *6 Hz*, Ar*H*); 3.34 (q, 2H, *J* = *6 Hz*, N—C*H*$_2$—CH_3); 1.20 (t, 3H, *J* = *6 Hz*, NCH_2—C*H*$_3$). ^{13}CNMR Spectrum δ ppm (100 MHz, DMSO d_6): 168.25 (thiadiazole *C5*); 156.13 (thiadiazole *C2*); 152.69 (urea *C*=O); 141.34, 138.97, 129.12, 127.52, 126.01, 124.99, 120.31, 118.81 (Ar*C*); 40.58–39.33 (DMSO and N—*C*H_2—CH_3); 14.75 (NCH_2—*C*H_3). LR-MS (ESI) (*m/z*): calculated [M + H]+: 374.08, found: 374.10; calculated for [M - H]-: 372.07, found: 372.10.

1-(4-Chlorophenyl)−3-{4-[5-(*propylamino*)−1,3,4-*thiadiazol*-2-*yl*] phenyl}urea **10f**: Yield 70%; HPLC t_R (min): 18.73; m.p. 228–229 °C; FTIR (cm^{-1}): 3290 (NH str.), 1633 (C=O); ^{1}HNMR Spectrum δ ppm (400 MHz, DMSO d_6): 9.12 and 9.02 (s, 2H, N*H*, urea); 8.51 (s, 1H, -N*H*—CH_3); 7.82 (d, 2H, *J* = *8.8 Hz*, Ar*H*); 7.72 (d, 2H, *J* = *8.8 Hz*, Ar*H*); 7.51 (d, 2H, *J* = *8.8 Hz*, Ar*H*); 7.40 (d, 2H, *J* = *8.8 Hz*, Ar*H*); 4.33 (t, 2H, NH—C*H*$_2$—C_2H_5); 1.74–1.64 (m, 2H, $NHCH_2$—C*H*$_2$—CH_3); 1.12 (t, 3H, *J* = *7.2 Hz*, NHC_2H_4—C*H*$_3$). ^{13}CNMR Spectrum δ ppm (100 MHz, DMSO d_6): 167.96 (thiadiazole *C5*); 155.54 (thiadiazole *C2*); 152.22 (urea *C*=O); 140.87, 138.52, 128.61, 127.00, 125.48, 124.49, 119.80, 118.31 (Ar*C*); 46.59 (NH—C*H*$_2$—C_2H_5); 40.09–38.84 (DMSO and

NHCH$_2$—CH$_2$—CH$_3$); 11.38 (NHC$_2$H$_4$—CH$_3$). LR-MS (ESI) (*m/z*): calculated [M + H]+: 388.10, found: 388.05; calculated for [M - H]-: 386.09, found: 386.15.

4.1.4. General procedure for the synthesis of target compounds 11a–f

About 1 mmol of compounds**7a–f** dissolved in 10 ml of NaOH, 2 N and heated in a water bath for about 4 h. The reaction was then cooled and the excess amount of NaOH was neutralized with HCl, 5% and the precipitated product was filtered off, washed, and crystallized with ethanol.

4.1.4.1. 1-(4-(4-Methyl-5-thioxo-4,5-dihydro-1H-1,2,4-triazol-3-yl)phenyl)−3-phenylurea 11a. White solid; yield 30%; HPLC t_R (min): 4.61; m.p. 297–299 °C; FTIR (cm^{-1}): 3273, 3196, 3111 (NH str.), 1703 (C=O), 1232 (C=S). ^{1}HNMR Spectrum δ ppm (400 MHz, DMSO d$_6$): 13.86 (s, 1H, N*H* triazole); 9.02 and 8.79 (s, 2H, urea N*H*); 7.66 (s, 4H, Ar-*H*); 7.47 (d, 2H, *J = 8.0 Hz*, Ar*H*); 7.31 (d, 2H, *J = 7.6 Hz*, Ar*H*); 7.00 (t, 1H, Ar*H*); 3.55 (s, 3H, N—C*H*$_3$). ^{13}CNMR Spectrum δ ppm (100 MHz, DMSO d$_6$): 167.29 (*C* = *S*); 152.73 (urea *C*=O); 151.45 (triazole *C3*); 142.25, 138.88, 129.91, 129.14, 126.13, 120.38, 119.65, 118.54, 113.86, 112.82 (Ar*C*); 32.14 (N—*C*H$_3$). LR-MS (ESI) (*m/z*): calculated [M + H]$^+$: 326.11, found: 326.10; calculated for [M - H]$^-$: 324.09, found: 324.15.

4.1.4.2. 1-Phenyl-3-(4-(4-propyl-5-thioxo-4,5-dihydro-1H-1,2,4-triazol-3-yl)phenyl)urea 11c. White solid; yield 27%; HPLC t_R (min): 7.41; m.p. 288 °C; FTIR (cm^{-1}): 3356 (NH str.), 1697 (C=O), 1260 (C=S). ^{1}HNMR Spectrum δ ppm (400 MHz, DMSO d$_6$): 13.86 (s, 1H, NH triazole); 9.01 and 8.79 (s, 2H, urea NH); 7.62 (dd, 4H, *J = 8.8 Hz,* Ar-H); 7.49 (d, 2H, *J = 7.6 Hz*, ArH); 7.31 (d, 2H, *J = 7.6 Hz*, ArH); 7.00 (t, 1H, *J = 7.6 Hz,* ArH); 4.02 (t, 2H, *J = 7.6 Hz,* NH—C*H*$_2$—C$_2$H$_5$); 1.60–1.55 (m, 2H, NHCH$_2$—C*H*$_2$—CH$_3$); 0.74 (t, 3H, *J = 7.2 Hz*, NHC$_2$H$_4$—C*H*$_3$). ^{13}CNMR Spectrum δ ppm (100 MHz, DMSO d6): 166.94 (C=S); 152.31 (urea C=O); 151.14 (triazole C3); 141.92, 139.37, 129.23, 128.80, 122.08, 119.10, 118.33, 118.00 (ArC); 45.13 (NH—*C*H$_2$—C$_2$H$_5$); 20.99 (NHCH$_2$—*C*H$_2$—CH$_3$); 10.69 (NHC$_2$H$_4$—*C*H$_3$). LR-MS (ESI) (*m/z*): calculated [M + H]$^+$: 355.15, found: 355.15; calculated for [M - H]$^-$: 352.12, found: 352.15.

4.1.4.3. 1-(4-Chlorophenyl)−3-(4-(4-methyl-5-thioxo-4,5-dihydro-1H-1,2,4-triazol-3-yl)phenyl)urea 11d. White solid; yield 48%; HPLC t_R (min): 5.28; m.p. 308–309 °C; FTIR (cm^{-1}): 3283 (NH str.), 1707 (C=O), 1233 (C=S). ^{1}HNMR Spectrum δ ppm (400 MHz, DMSO d$_6$): 13.86 (s, 1H, N*H* triazole); 9.06 and 8.94 (s, 2H, urea N*H*); 7.71–7.55 (m, 4H, Ar*H*); 7.51 (d, 2H, *J = 8.8 Hz*, Ar*H*); 7.35 (d, 2H, *J = 8.8 Hz*, Ar*H*); 3.60 (s, 3H, N—C*H*$_3$). ^{13}CNMR Spectrum δ ppm (100 MHz, DMSO d$_6$): 166.74 (*C*=S); 152.06 (urea *C*=O); 150.89 (triazole *C3*); 141.86, 139.28, 129.34, 129.14, 128.73, 122.02, 118.91, 118.26, 117.84, 112.91, 112.25 (Ar*C*); 31.56 (N—*C*H$_3$). LR-MS (ESI) (*m/z*): calculated [M + H]$^+$: 360.07, found: 360.10; calculated for [M - H]$^-$: 358.05, found: 358.10.

4.1.4.4. 1-(4-Chlorophenyl)−3-(4-(4-propyl-5-thioxo-4,5-dihydro-1H-1,2,4-triazol-3-yl)phenyl)urea 11f. White solid; yield 59%; HPLC t_R (min): 13.16; m.p. 265–267 °C; FTIR (cm^{-1}): 3335, 3254 (NH str.), 1716 (C=O), 1235 (C = S). ^{1}HNMR Spectrum δ ppm (400 MHz, DMSO d$_6$): 14.01 (s, 1H, NH triazole); 9.19 and 9.08 (s, 2H, urea N*H*); 7.76 (dd, 4H, *J = 8.8 Hz*, Ar*H*); 7.65 (d, 2H, *J = 8.8 Hz*, Ar*H*); 7.50 (d, 2H, *J = 8.8 Hz*, Ar*H*); 4.16 (t, 2H, *J = 7.6 Hz,* NH—C*H*$_2$—C$_2$H$_5$); 1.74–1.68 (m, 2H, NHCH$_2$—C*H*$_2$—CH$_3$); 0.88 (t, 3H, *J = 7.6 Hz*, NHC$_2$H$_4$—C*H*$_3$). ^{13}CNMR Spectrum δ ppm (100 MHz, DMSO d6): 167.44 (*C* = S); 152.76 (urea *C* = O); 151.62 (triazole *C3*); 142.27, 138.93, 129.84, 129.72, 129.14, 126.08, 130.34, 119.75, 118.60, 113.97, 112.93 (Ar*C*); 45.63 (NH—*C*H$_2$—C$_2$H$_5$); 21.49 (NHCH$_2$—*C*H$_2$—CH$_3$); 11.19 (NHC$_2$H$_4$—*C*H$_3$). LR-MS (ESI) (*m/z*): calculated [(M +2)+ H]$^+$: 390.10, found: 390.10; calculated for [M - H]$^-$: 386.09, found: 386.15.

4.1.5. General procedure for the synthesis of the compounds 11g–l

To a solution of compounds **4a–c** (1 mmol) in dichloromethane (5 mL), the appropriate isocyanate derivatives (1 mmol) were added. The reaction mixture was stirred for 8 h at room temperature, and then the solvent evaporated. The solid product obtained upon evaporating the solvent crystallized from ethanol to obtain compounds **11g–l**.

4.1.5.1. 1-(4-(4-Methyl-5-thioxo-4,5-dihydro-1H-1,2,4-triazol-3-yl)phenyl)−3-(3-(trifluoromethyl)phenyl)urea 11 g. White solid; yield 61%; HPLC t_R (min): 13.18; m.p. 320–322 °C; FTIR (cm^{-1}): 3336 (NH str.); 1657 (C=O), 1219 (C=S). ^{1}HNMR Spectrum δ ppm (400 MHz, DMSO d$_6$): 13.92 (s, 1H, N*H* triazole); 9.22 and 9.20 (s, 2H, N*H*, urea); 8.09 (s, 1H, Ar*H*); 7.77–7.57 (m, 6H, Ar*H*); 7.40 (d, 1H, *J = 7.6 Hz*, Ar*H*); 3.66 (s, 3H, N—C*H*$_3$). ^{13}CNMR Spectrum δ ppm (100 MHz, DMSO d$_6$): 162.76 (triazole *C*=S); 152.83 (urea *C*=O); 151.80 (triazole *C*3); 142.10, 140.79, 130.43, 130.17 (Ar*C*); 129.86, 126.01, 123.31 (*C*F$_3$); 129.72, 122.49, 119.86, 118.83, 118.71, 114.78 (Ar*C*); 32.13 (N—*C*H$_3$). LR-MS (ESI) (*m/z*): calculated [M + Na]$^+$: 416.08, found: 416.10; calculated for [M - H]$^-$: 392.08, found: 392.10.

4.1.5.2. 1-(4-(4-Ethyl-5-thioxo-4,5-dihydro-1H-1,2,4-triazol-3-yl)phenyl)−3-(3-(trifluoromethyl)phenyl)urea 11 h. White solid; yield 58%; HPLC t_R (min): 13.16; m.p. 227–229 °C; FTIR (cm^{-1}): 3364 (NH str.); 1703 (C=O), 1233 (C=S). ^{1}HNMR Spectrum δ ppm (400 MHz, DMSO d$_6$): 13.88 (s, 1H, N*H* triazole); 9.18 and 9.16 (s, 2H, N*H*, urea); 8.04 (s, 1H, Ar*H*); 7.69–7.54 (m, 6H, Ar*H*); 7.35 (d, 1H, *J = 6.8 Hz*, Ar*H*); 4.07 (q, 2H, *J = 6.8 Hz*, N—C*H*$_2$—CH$_3$); 1.19 (t, 3H, *J = 6.8 Hz*, NCH$_2$—C*H*$_3$). ^{13}CNMR Spectrum δ ppm (100 MHz, DMSO d$_6$): 167.12 (triazole *C*=S); 152.84 (urea *C*=O); 151.48 (triazole *C*3); 142.14, 140.80, 130.43, 130.18 (Ar*C*); 129.86, 126.01, 123.31 (*C*F$_3$); 129.72, 122.49, 119.85, 118.86, 114.78 (Ar*C*); 40.57–39.32 (DMSO and N—*C*H$_2$—CH$_3$); 13.91 (NCH$_2$—*C*H$_3$). LR-MS (ESI) (*m/z*): calculated [M + Na]$^+$: 430.09, found: 430.10; calculated for [M - H]$^-$: 406.10, found: 406.20.

4.1.5.3. 1-(4-(4-Propyl-5-thioxo-4,5-dihydro-1H-1,2,4-triazol-3-yl)phenyl)−3-(3-(trifluoromethyl)phenyl)urea 11i. White solid; yield 63%; HPLC t_R (min): 23.26; m.p. 206–208 °C; FTIR (cm^{-1}): 3310 (NH str.); 1705 (C=O), 1233 (C=S). ^{1}HNMR Spectrum δ ppm (400 MHz, DMSO d$_6$): 13.88 (s, 1H, NH triazole); 9.18 and 9.15 (s, 2H, urea NH); 8.04 (s, 1H, Ar*H*); 7.73–7.52 (m, 6H, Ar*H*); 7.34 (d, 1H, *J = 6.8 Hz*, Ar*H*); 4.02 (t, 2H, *J = 6.8 Hz*, N—C*H*$_2$—C$_2$H$_5$); 1.60–1.55 (m, 2H, NCH$_2$—C*H*$_2$—CH$_3$); 0.74 (t, 3H, *J = 7.2 Hz*, NC$_2$H$_4$—C*H*$_3$). ^{13}CNMR Spectrum δ ppm (100 MHz, DMSO d6): 166.97 (*C*=S); 152.34 (urea *C*=O); 151.09 (triazole *C3*); 141.58, 140.29, 129.92, 129.22 (Ar*C*); 129.68, 125.51, 122.80 (*C*F$_3$); 121.98, 119.47, 118.33, 114.29, 114.24 (Ar*C*); 45.13 (N—*C*H$_2$—C$_2$H$_5$); 20.98 (NCH$_2$—*C*H$_2$—CH$_3$); 10.67 (NC$_2$H$_4$—*C*H$_3$). LR-MS (ESI) (*m/z*): calculated [M + Na]$^+$: 444.11, found: 444.15; calculated for [M - H]$^-$: 420.11, found: 420.15.

4.1.5.4. 1-(4-(4-Methyl-5-thioxo-4,5-dihydro-1H-1,2,4-triazol-3-yl)phenyl)−3-(4 (trifluoromethyl)phenyl)urea 11j. White solid; yield 70%; HPLC t_R (min): 12.73; m.p. 308–310 °C; FTIR (cm^{-1}): 3342 (NH str.); 1663 (C=O), 1240 (C=S). ^{1}HNMR Spectrum δ ppm (400 MHz, DMSO d$_6$): 13.87 (s, 1H, N*H* triazole); 9.23 and 9.16 (s, 2H, urea N*H*); 7.70–7.65 (m, 8H, Ar*H*); 3.55 (s, 3H, N—C*H*$_3$). ^{13}CNMR Spectrum δ ppm (100 MHz, DMSO d$_6$): 167.75 (triazole *C*=S); 152.61 (urea *C*=O); 151.79 (triazole *C*3); 143.65, 142.02, 129.73, 126.60 (Ar*C*); 129.02, 126.56, 123.64 (*C*F$_3$); 122.97, 122.66, 122.34, 122.02, 120.94, 119.90, 118.69, 118.50 (Ar*C*); 32.12 (N—*C*H$_3$). LR-MS (ESI) (*m/z*): calculated [M + Na]$^+$: 416.08, found: 416.10; calculated for [M - H]$^-$: 392.08, found: 392.10.

4.1.5.5. 1-(4-(4-Ethyl-5-thioxo-4,5-dihydro-1H-1,2,4-triazol-3-yl)phenyl)−3-(4-(trifluoromethyl)phenyl)urea 11k. White solid; yield 62%; HPLC t_R (min): 16.01; m.p. 242–244 °C; FTIR (cm^{-1}): 3337, 3275 (NH

str.); 1703 (C=O), 1242 (C = S). ^{1}HNMR Spectrum δ ppm (400 MHz, DMSO d_6): 13.88 (s, 1H, N*H* triazole); 9.23 and 9.16 (s, 2H, urea N*H*); 7.70–7.61 (m, 8H, Ar*H*); 4.07 (q, 2H, *J* = 6.8 Hz, N—C*H*$_2$—CH$_3$); 1.79 (t, 3H, *J* = *6.4 Hz*, NCH$_2$—C*H*$_3$). ^{13}CNMR Spectrum δ ppm (100 MHz, DMSO d_6): 167.12 (triazole *C*=S); 152.62 (urea *C*=O); 151.46 (triazole *C*3); 143.67, 142.08, 129.75, 126.61, 126.57 (Ar*C*); 126.34, 123.64, 122.33 (*C*F$_3$); 122.65, 119.90, 118.82, 118.50 (Ar*C*); 40.58–39.33 (DMSO and N—*C*H$_2$—CH$_3$); 13.90 (NCH$_2$—*C*H$_3$). LR-MS (ESI) (*m/z*): calculated [M + Na]$^+$: 430.09, found: 430.15; calculated for [M - H]$^-$: 406.10, found: 406.15.

4.1.5.6. 1-(4-(4-Propyl-5-thioxo-4,5-dihydro-1H-1,2,4-triazol-3-yl)phenyl)−3-(4-(trifluoromethyl)phenyl)urea 11l. White solid; yield 58%; HPLC t_R (min): 22.24; m.p. 208–210 °C; FTIR (cm^{-1}): 3266, 3198 (NH str.); 1699 (C=O), 1240 (C=S). ^{1}HNMR Spectrum δ ppm (400 MHz, DMSO d_6): 13.88 (s, 1H, N*H* triazole); 9.23 and 9.15 (s, 2H, urea N*H*); 7.68–7.61 (m, 8H, Ar*H*); 4.02 (t, 2H, *J* = *7.2 Hz*, N—C*H*$_2$—C$_2$H$_5$); 1.60–1.55 (m, 2H, NCH$_2$—C*H*$_2$—CH$_3$); 0.74 (t, 3H, *J* = *7.2 Hz*, NC$_2$H$_4$—C*H*$_3$). ^{13}CNMR Spectrum δ ppm (100 MHz, DMSO d6): 167.47 (triazole C=S); 152.64 (urea C=O); 151.59 (triazole C3); 143.68, 142.04, 129.78 (ArC); 129.03, 126.34, 123.65 (CF$_3$); 126.61, 122.65, 122.34, 120.03, 118.79, 118.51 (ArC); 45.64 (N—*C*H$_2$—C$_2$H$_5$); 21.50 (NCH$_2$—*C*H$_2$—CH$_3$); 11.20 (NC$_2$H$_4$—*C*H$_3$). LR-MS (ESI) (*m/z*): calculated [M + Na]$^+$: 444.11, found: 444.15; calculated for [M - H]$^-$: 420.11, found: 420.15.

4.2. Biological evaluation

4.2.1. In vitro VEGFR-2 kinase assays

4.2.1.1. Screening of compounds against VEGFR-2. All screening experiments of our 22 newly synthesized compounds and positive controls (sorafenib and staurosporin) at one concentration (10 μM) were completed by Reaction Biology Europe (RBE) GMHB (Freiburg, Germany). A radiometric protein kinase assay (33PanQinase® Activity Assay) was used for measuring the kinase activity of the protein kinase. All kinase assays were performed in 96-well ScintiPlatesTM from Perkin Elmer (Boston, MA, USA) in a 50 μl reaction volume. The assay for the protein kinase contained 70 mM HEPES-NaOH pH 7.5, 3 mM $MgCl_2$, 3 mM $MnCl_2$, 3 μM Na-orthovanadate, 1.2 mM DTT, 50 μg/ml PEG_{20000}, ATP (corresponding to the apparent ATP-Km of the kinase, 1 μM), [γ−^{33}P]-ATP (approx. 8 × 1005 cpm per well), VEGFR-2, and substrate Poly(Glu,Tyr) 4:1 (2.5 ng/μL). The mixtures were incubated at 30 °C for 60 min and the reaction was terminated with the addition of 2% (v/v) H_3PO_4. Plates were washed with 0.876% (w/v) NaCl solution and using a microplate scintillation counter (Microbeta, Wallac) incorporation of ^{33}Pi (counting of "cpm") was determined. The residual activity (in%) for each compound well was calculated by using the following formula:

$$\text{Res.Activity}(\%) = 100 \times [(\text{cpmofcompound} - - \text{lowcontrol}) / (\text{highcontrol} - - \text{lowcontrol})]$$

where "low control" defined as the average cpm of three wells that contains the reactiom mixture except the VEGFR-2 and "high control" is the average cpm of three wells that contains the reactiom mixture except the tested derivative ($n = 3$)

4.2.1.2. Determination of the IC_{50} values of the most active compounds. The IC_{50} values of the most potent VEGFR-2 inhibitors having less than 30% residual activity at 10 μM in the screening assay were determined against VEGFR-2 by the well-established FRET-based Z′-Lyte assay as per the guidelines provided by the manufacturer (Thermo Fisher Scientific, Waltham,MA, USA). VEGFR-2 (KDR, PV3660, Thermo Fisher Scientific), Z'-LYTE™ Tyr 1 Peptide (PV3257, Thermo Fisher Scientific), 10 μM ATP, and different concentrations of the compounds **10c, 8a**, 11 g, or sorafenib as a positive control, were used in the reactions, which were conducted on 384-well plates. The final 10 μL Kinase Reaction consists of 0.5–11.7 ng KDR (VEGFR-2) and 2 μM Tyr 01 in 50 mM HEPES pH 7.5, 0.01% BRIJ-35, 10 mM $MgCl_2$, 1 mM EGTA. After an hour of incubation at room temperature, a stop solution was used to quench all of the reactions. Utilizing a BioTek FLx800 (BioTek, Winooski, VT, USA) device, the fluorescence signal at 445 nm (coumarin) and 520 nm (fluorescein), which indicates the reaction's kinase inhibition and/or peptide substrate cleavage state, was recorded. Data were analyzed by Graphpad Prism 8.01 (Graphpad Software, Inc) and the IC_{50} values were calculated by nonlinear regression of log concentration versus the% inhibition of phosphorylation.

4.2.2. In vitro anti-proliferative activity against normal and cancer cells

Breast carcinoma (MCF-7) cell line, triple negative human breast adenocarcinoma (MDA-MB-231) cell line and noncancerous fibroblast cells (L929) were utilized for the MTT assay [33]. In a humidified environment with 5% CO_2 in the air, cells were maintained in Dulbecco's modified Eagle's medium (DMEM, Invitrogen) or RPMI-1640 supplemented with 10% FBS, 2 mM L-glutamine, 100 U/mL penicillin, and 100 μg/mL streptomycin. To determine the cell viability cells were plated onto 96-well plates (1 × 104 cells/well). The cells were treated with different concentrations (0, 0.1, 1, 10, 100, and 1000 μM) of synthesized compounds or reference sorafenib and the plates were then left to incubate for 24 h. After the incubation, cells were washed with PBS and added to 100 μL DMEM/RPMI-1640. A total of 10 μL of the MTT (Vybrant, Invitrogen) labeling reagent was added to each well and incubated for 4 h in a humidified atmosphere at 37 °C incubator with 5% CO_2 in the air. Following the incubation, in order to dissolve the formazan precipitate, 100 μL of the SDS buffer was added to each well. Then absorbance was measured by a microplate reader at 570 nm and carried out in triplicate of each assay.

4.2.3. Annexin-V/PI assay with flow cytometry

MCF-7 and MDA-MB-231 cells (1 × 10^6 cells/well) were seeded in 6-well plates. Compounds **9d** and **8a** (for MCF-7, 9.37 and 1.96 μM and for MDA-MB-231, 5.83 and 3.48 μM, respectively) treated with cells for 24 h. After incubation, cells were harvested with trypsin-EDTA and washed with PBS. The cells were then suspended in 500 μL of cold PBS. Commercial kit was used for Annexin-V measurement and the manufacturer's protocol was followed (BD Pharmingen, AB-2,869,082). 5 μL of Annexin-V and 5 μL of propidium iodide (PI) were added to the suspended cells, and 500 μL of binding buffer was added and incubated for 20 min at room temperature in the dark. A flow cytometer (Novocyte, Agilent) was used to analyze AnnexinV/PI binding in the cells after incubation [34]. A total of 25.000 cells were counted in the device and their positions were determined according to the FSC/SSC method. AnnexinV/PI binding was calculated on the basis of gate coupled in control cells.

4.3. In silico studies

4.3.1. Molecular modeling

The crystal structure of VEGFR-2 protein complexed with the angiogenesis inhibitor Sorafenib (PDB ID: 4ASD; resolution: 2.03 Å) [35] was retrieved from the Protein Data Bank. The protein preparation was carried out using the BioVia (2016) Discovery Studio program.

Within the scope of the protein preparation protocol inhibitor, water molecules and irrelevant ions were removed. The missing hydrogen atoms were added according to the protonation state of the receptor at a pH of 7.4, maintaining the default values of 0.145 and 10 for the ionic strength and the dielectric constant, respectively. Finally, the protein preparation protocol was employed, utilizing the "*Clean Geometry*" toolkit in Discovery Studio (v. 4.5) software to prepare and minimize the receptor before docking. Following the protein preparation stage, all ligand structures were drawn, and the geometry of the ligands was optimized using the Discovery Studio prepare ligand protocol.

Proceeding the ligands preparations, we use AutoDock Tools (ADT) (http://mgltools.scripps. edu/downloads) graphical user interface program to produce the input filers such as the grid parameter file (gpf) the docking parameter file (dpf) [36]. The grid box size set to 60, 60, and 60 Å, and the x, y, and z coordinates for the grid center were adjusted to 26.53, 21.30, and 17.55, respectively. Also, the space of the grid box was maintained at 0.375 Å. Finally, the AutoDock4 docking program [37] employed for docking of ligands with the preference of the Lamarckian Genetic Algorithm (LGA) for docking simulation; other parameters of LGA remain at default values, except for energy evaluations, which was adjusted to 25,000, 000.

AutodockTools 1.5.6 interface program was used to prepare input files for docking. Autodock 4.2 molecular docking program was employed for all docking studies. The Discovery Studio visualization program was utilized to generate all the 2D and 3D pictures. In all silico studies conducted using the Dell Precision workstation.

4.3.2. Determination of in silico physicochemical and pharmacokinetic properties

Pharmacokinetic and physicochemical properties of the synthesized compounds and control compounds sorafenib and staurosporine was investigated using SwissADME website (http://www.swissadme.ch/index.php). Lipophilicty of the compounds predicted by BOILED-Egg model of SwissADME (the WLOGP vs. TPSA) for the synthesized compounds and controls [29]. Bioavailability radar, which is a plot of six different physicochemical properties, including size, polarity, lipophilicity, solubility, flexibility, and saturation were also constructed by SwissADME model [38].

CRediT authorship contribution statement

Mohammad Musa Shirzad: Investigation, Funding acquisition, Writing – original draft. **Necla Kulabaş:** Investigation, Writing – review & editing. **Ömer Erdoğan:** Investigation, Writing – review & editing. **Özge Çevik:** Investigation, Writing – review & editing. **Damla Dere:** Investigation, Writing – review & editing. **Kemal Yelekçi:** Investigation, Writing – review & editing. **Özkan Danış:** Conceptualization, Methodology, Funding acquisition, Investigation, Writing – original draft. **İlkay Küçükgüzel:** Conceptualization, Methodology, Funding acquisition, Investigation, Writing – original draft.

Declaration of Competing Interest

The authors declare the following financial interests/personal relationships which may be considered as potential competing interests: Ozkan Danis reports a relationship with Marmara University that includes: funding grants.

Data availability

Data will be made available on request.

Acknowledgments

This work was supported by Marmara University Scientific Research Fund, Türkiye through Project FENC-DRP-170419-0127.

Supplementary materials

Supplementary material associated with this article can be found, in the online version, at doi:10.1016/j.molstruc.2023.136448.

References

[1] H.A. Assi, K.E. Khoury, H. Dbouk, L.E. Khalil, T.H. Mouhieddine, N.S. El Saghir, Epidemiology and prognosis of breast cancer in young women, J. Thorac. Dis. 5 (Suppl 1) (2013) S2–S8, https://doi.org/10.3978/j.issn.2072-1439.2013.05.24.
[2] H. Zahreddine, K.L. Borden, Mechanisms and insights into drug resistance in cancer, Front. Pharmacol. 4 (2013) 28, https://doi.org/10.3389/fphar.2013.00028.
[3] S.J. Modi, V.M. Kulkarni, Vascular endothelial growth factor receptor (VEGFR-2)/KDR inhibitors: medicinal chemistry perspective, Med. Drug Dis. 2 (2019), 100009, https://doi.org/10.1016/j.medidd.2019.100009.
[4] A. Hassan, M. Badr, D. Abdelhamid, H.A. Hassan, M.A.S. Abourehab, G.E.A. Abuo-Rahma, Design, synthesis, *in vitro* antiproliferative evaluation and *in silico* studies of new VEGFR-2 inhibitors based on 4-piperazinylquinolin-2(1H)-one scaffold, Bioorg. Chem. 120 (2022), 105631, https://doi.org/10.1016/j.bioorg.2022.105631.
[5] P. Cohen, Protein kinases-the major drug targets of the twenty-first century? Nat. Rev. Drug Discov. 1 (2002) 309–315, https://doi.org/10.1038/nrd773.
[6] G.K. Kanev, C. de Graaf, I.J.P. de Esch, et al., The landscape of atypical and eukaryotic protein kinases, Trends Pharmacol. Sci. 40 (2019) 818–832, https://doi.org/10.1016/j.tips.2019.09.002.
[7] R. Roskoski, Small molecule inhibitors targeting the EGFR/ErbB family of protein-tyrosine kinases in human cancers, Pharmacol. Res. 139 (2019) 395–411, https://doi.org/10.1016/j.phrs.2018.11.014.
[8] S. Guo, L.S. Colbert, T.Z. McCloten, R.R. Gonzalez-Perez, Regulation of Angiogenesis in Human Cancer Via Vascular Endothelial Growth Factor Receptor-2 (VEGFR-2), Tumor Angiogenesis, InTech, 2012, https://doi.org/10.5772/27370.
[9] X. Wang, A.M. Bove, G. Simone, B. Ma, Molecular bases of VEGFR-2-mediated physiological function and pathological role, Front. Cell. Dev. Biol. 8 (2020), 599281, https://doi.org/10.3389/fcell.2020.599281. Published 2020 Nov 16.
[10] L. Nakopoulou, K. Stefanaki, E. Panayotopoulou, et al., Expression of the vascular endothelial growth factor receptor-2/Flk-1 in breast carcinomas: correlation with proliferation, Hum. Pathol. 33 (2002) 863–870, https://doi.org/10.1053/hupa.2002.126879.
[11] R. Roskoski, Properties of FDA-approved small molecule protein kinase inhibitors: a 2021 update, Pharmacol. Res. 165 (2021), 105463, https://doi.org/10.1016/j.phrs.2021.105463.
[12] P. Shiri, S.:. Ramezanpour, A.M. Amani, W. Dehaen, A patent review on efficient strategies for the total synthesis of pazopanib, regorafenib and lenvatinib as novel anti-angiogenesis receptor tyrosine kinase inhibitors for cancer therapy, Mol. Divers. 26 (2022) 2981–3002, https://doi.org/10.1007/s11030-022-10406-8.
[13] X.J. Liu, H.C. Zhao, S.J. Hou, et al., Recent development of multi-target VEGFR-2 inhibitors for the cancer therapy, Bioorg. Chem. 133 (2023), 106425, https://doi.org/10.1016/j.bioorg.2023.106425.
[14] R. Roskoski, Classification of small molecule protein kinase inhibitors based upon the structures of their drug-enzyme complexes, Pharmacol. Res. 103 (2016) 26–48, https://doi.org/10.1016/j.phrs.2015.10.021.
[15] A.C. Dar, K.M. Shokat, The evolution of protein kinase inhibitors from antagonists to agonists of cellular signaling, Annu. Rev. Biochem. 80 (2011) 769–795, https://doi.org/10.1146/annurev-biochem-090308-173656.
[16] W.M. Eldehna, A.M. El Kerdawy, G.H. Al-Ansary, S.T. Al-Rashood, M.M. Ali, A. E. Mahmoud, Type IIA - Type IIB protein tyrosine kinase inhibitors hybridization as an efficient approach for potent multikinase inhibitor development: design, synthesis, anti-proliferative activity, multikinase inhibitory activity and molecular modeling of novel indolinone-based ureides and amides, Eur. J. Med. Chem. 163 (2019) 37–53, https://doi.org/10.1016/j.ejmech.2018.11.061.
[17] X.R. Wang, S. Wang, W.B. Li, et al., Design, synthesis and biological evaluation of novel 2-(4-(1H-indazol-6-yl)-1H-pyrazol-1-yl)acetamide derivatives as potent VEGFR-2 inhibitors, Eur. J. Med. Chem. 213 (2021), 113192, https://doi.org/10.1016/j.ejmech.2021.113192.
[18] C. Pottier, M. Fresnais, M. Gilon, G. Jérusalem, R. Longuespée, N.E. Sounni, Tyrosine kinase inhibitors in cancer: breakthrough and challenges of targeted therapy, Cancers 12 (2020) 731, https://doi.org/10.3390/cancers12030731 (Basel)Published 2020 Mar 20.
[19] O.M. Soltan, M.E. Shoman, S.A. Abdel-Aziz, A. Narumi, H. Konno, M. Abdel-Aziz, Molecular hybrids: a five-year survey on structures of multiple targeted hybrids of protein kinase inhibitors for cancer therapy, Eur. J. Med. Chem. 225 (2021), 113768, https://doi.org/10.1016/j.ejmech.2021.113768.
[20] E. Tatar, S. Yaldız, N. Kulabaş, E. Vanderlinden, L. Naesens, İ. Küçükgüzel, Synthesis and structure-activity relationship of L-methionine-coupled 1,3,4-thiadiazole derivatives with activity against influenza virus, Chem. Biol. Drug Des. 99 (2022) 398–415, https://doi.org/10.1111/cbdd.13995.
[21] S. Aydın, N. Kaushik-Basu, S. Özbaş-Turan, J. Akbuğa, T.P. Mega, O.R. Orun, K.B. A. Gurukumar, K.Ş. Güniz, Synthesis of 1-aroyl-3,5-dimethyl-1H-pyrazoles as Anti-HCV and anticancer agents, Lett. Drug Des. Discov. 11 (2014) 121–131, https://doi.org/10.2174/15701808113109990069.

[22] N. Kulabaş, E. Tatar, Ö. Bingöl Özakpınar, et al., Synthesis and antiproliferative evaluation of novel 2-(4H-1,2,4-triazole-3-ylthio)acetamide derivatives as inducers of apoptosis in cancer cells, Eur. J. Med. Chem. 121 (2016) 58–70, https://doi.org/10.1016/j.ejmech.2016.05.017.
[23] İ. Demirbolat, N. Kulabaş, M. Gürboğa, Ö.B. Özakpınar, G. Çiftçi, K. Yelekçi, L. Jianyang, J. Per-Johan, Ö. Danış, A. Ogan, İ. Küçükgüzel, Synthesis and evaluation of antiproliferative and mPGES-1 inhibitory activities of novel carvacrol-triazole conjugates, Org. Comm. 15 (2022) 356–377, https://doi.org/10.25135/acg.oc.142.2212.2651.
[24] B. Bülbül, K. Ding, C.G. Zhan, et al., Novel 1,2,4-triazoles derived from Ibuprofen: synthesis and *in vitro* evaluation of their mPGES-1 inhibitory and antiproliferative activity, Mol. Divers. (2022), https://doi.org/10.1007/s11030-022-10551-0.
[25] İ. Küçükgüzel, S. Rollas, M. Ülgen, Synthesis and characterization of some thiourea derivatives from 1,2,4-triazolin3-3-thiones, Marmara Pharm. J. 10 (1994) 17–25, https://doi.org/10.12991/mpj.52639.
[26] G. Erensoy, K. Ding, C. Zhan, G. Çiftçi, K. Yelekçi, M. Duracık, Ö.B. Özakpınar, E. Aydemir, Z.N. Yılmaz, F. Şahin, N. Kulabaş, E. Tatar, İ. Küçükgüzel, Synthesis, *in vitro* and *in silico* studies on novel 3-aryloxymethyl-5-[(2-*oxo*-2-*arylethyl*)*sulfanyl*]-1,2,4-triazoles and their oxime derivatives as potent inhibitors of mPGES-1, J. Mol. Struct. 1272 (2023), 134154, https://doi.org/10.1016/j.molstruc.2022.134154.
[27] L. Garuti, M. Roberti, G. Bottegoni, M. Ferraro, Diaryl urea: a privileged structure in anticancer agents, Curr. Med. Chem. 23 (2016) 1528–1548, https://doi.org/10.2174/0929867323666160411142532.
[28] M. Sun, X. Wu, J. Chen, J. Cai, M. Cao, M. Ji, Design, synthesis, and *in vitro* antitumor evaluation of novel diaryl ureas derivatives, Eur. J. Med. Chem. 45 (2010) 2299–2306, https://doi.org/10.1016/j.ejmech.2010.02.005.
[29] A. Daina, V.A. Zoete, BOILED-egg to predict gastrointestinal absorption and brain penetration of small molecules, ChemMedChem 11 (2016) 1117–1121, https://doi.org/10.1002/cmdc.201600182.
[30] A. Daina, O. Michielin, V. Zoete, SwissADME: a free web tool to evaluate pharmacokinetics, drug-likeness and medicinal chemistry friendliness of small molecules, Sci. Rep. 7 (2017) 42717, https://doi.org/10.1038/srep42717. Published 2017 Mar 3.
[31] C.A. Lipinski, F. Lombardo, B.W. Dominy, P.J. Feeney, Experimental and computational approaches to estimate solubility and permeability in drug discovery and development settings, Adv. Drug Deliv. Rev. 46 (2001) 3–26, https://doi.org/10.1016/s0169-409x(00)00129-0.
[32] D.F. Veber, S.R. Johnson, H.Y. Cheng, B.R. Smith, K.W. Ward, K.D. Kopple, Molecular properties that influence the oral bioavailability of drug candidates, J. Med. Chem. 45 (2002) 2615–2623, https://doi.org/10.1021/jm020017n.
[33] T. Mosmann, Rapid colorimetric assay for cellular growth and survival: application to proliferation and cytotoxicity assays, J. Immunol. Methods 65 (1983) 55–63, https://doi.org/10.1016/0022-1759(83)90303-4.
[34] D. Uslu, B.I. Abas, G.M. Demirbolat, O. Cevik, Effect of platelet exosomes loaded with doxorubicin as a targeted therapy on triple-negative breast cancer cells, Mol. Divers. (2022), https://doi.org/10.1007/s11030-022-10591-6.
[35] M. McTigue, B.W. Murray, J.H. Chen, Y.L. Deng, J. Solowiej, R.S. Kania, Molecular conformations, interactions, and properties associated with drug efficiency and clinical performance among VEGFR TK inhibitors, Proc. Natl. Acad. Sci. U. S. A. 109 (2012) 18281–18289, https://doi.org/10.1073/pnas.1207759109.
[36] K. Yelekçi, S.S. Erdem, Computational chemistry and molecular modeling of reversible MAO inhibitors, Methods Mol. Biol. 2558 (2023) 221–252, https://doi.org/10.1007/978-1-0716-2643-6_17.
[37] G.M. Morris, R. Huey, W. Lindstrom, M.F. Sanner, R.K. Belew, D.S. Goodsell, A. J. Olson, AutoDock4 and AutoDockTools4: automated docking with selective receptor flexibility, J. Comput. Chem. 16 (2009) 2785–2791, https://doi.org/10.1002/jcc.21256.
[38] T.J. Ritchie, P. Ertl, R. Lewis, The graphical representation of ADME-related molecule properties for medicinal chemists, Drug Discov. Today 16 (2011) 65–72, https://doi.org/10.1016/j.drudis.2010.11.002.